(TIJMS)

The International JOURNAL of MEDICINE and SCIENCES

VOL. 4 NO. 1 JUNE 2019

E-ISSN 2590-3713

Kulliyyah of Medicine & Health Sciences
Universiti Islam Antarabangsa Sultan Abdul Halim Mu'adzam Shah (UniSHAMS)

EDITORIAL BOARD

Kulliyyah of Medicine & Health Sciences, Universiti Islam Antarabangsa Sultan Abdul Halim Mu'adzam Shah,
09300 Kuala Ketil, Kedah Darul Aman.
tijms.editor@gmail.com

www.tijms.unishams.edu.my

Case Report

A DEADLY CASE OF CHOROIDAL METASTASIS

Brindha Gulendran*[1], Nazrah R [1], Rona Asnida N [2]

[1] Department of Ophthalmology, Hospital Selayang, 68100 Batu Caves, Selangor, Malaysia.
[2] Department of Ophthalmology, Universiti Kebangsaan Malaysia Medical Centre, Jalan Yaacob Latif, Bandar Tun Razak, 56000, Cheras, Kuala Lumpur, Malaysia.

ARTICLE INFO

Corresponding author:
Dr. Brindha Gulendran

Email address:
brindha12@hotmail.com

Received:
August 2018
Accepted for publication:
December 2018

Keywords:

sudden reduced vision,
exudative retinal detachment,
choroidal mass
advanced lung carcinoma,
metastasis

ABSTRACT

A case of 58-year-old Malay gentleman,a chronic smoker with underlying hypertension and diagnosed with smear positive tuberculosis, was referred for sudden onset of reduced vision in the left eye one month prior to presentation and after commencing anti-tuberculosis medications. Examination revealed right best corrected visual acuity (BCVA) of 6/9 and left BCVA was Counting Fingers(CF)1foot. Anterior segment examinations were normal. Funduscopy revealed left exudative retinal detachment superotemporally extending to the macula.The right fundus was normal. Calcification were present inferiorly. left Bscan showed a choroidal mass.A large heterogenously enhancing mass measuring 6.8 x 7.3 x 7.1 cm in the upper lobe of the right lung with a regular and spiculated margin was seen on CT TAP scan. with multiple small satellite nodules surrounding it. There also was multilevel bone metastases at cervical, thoracic, lumbar and sacral spine with soft tissue component causing multilevel spinal canal stenosis and nerve roots impingement. Final diagnosis was Stage 4 Lung carcinoma with distant metastases to spine, choroid, liver and lymph nodes. Patient was offered bronchoscopy for biopsy however he refused. Patient subsequently developed pneumonia and acute kidney injury secondary to poor oral intake and was treated with intravenous Ceftriaxone 2gm OD . Patient deteriorated and succumbed within a month of diagnosis of due to advanced lung carcinoma.

INTRODUCTION

Choroidal metastases is a rare occurrence and tend to occur in the advanced stages of cancer, where the mean survival is not expected to be more than 6 months [1]. It requires multidisciplinary care and should be among the differential in patients with malignancy who present with ocular symptoms [1]. The choroidal metastases are often asymptomatic and, thus, their diagnosis remains challenging. Their frequency might be underestimated due to the fact that most patients have advanced systemic disease which draws the attention away from ophthalmic examination unless it has caused severe visual impairment.

METHODS

Complete ophthalmological examination, blood investigation and imaging.

CASE REPORT

Mr MA, a 58-year-old Malay gentleman with underlying hypertension and dyslipidemia was referred from Internal Medicine department for sudden onset of blurring of left vision of one month duration. It was painless but progressively worsening. No floaters or flashes were noted. There was no prior history of trauma or red eyes; neither was there any significant past ocular history. His right vision was good. On further questioning, he initially presented to the emergency department 2 months prior with complaint of lower back pain. Patient was discharged with pain killer. His lower back pain worsened with associated numbness, weakness and acute urinary retention.

He sought treatment from a private hospital where a MRI spine was done. MRI revealed, aggressive lesion involving L4-S1 vertebrae with L3-L4 left paravertebral mass with intraspinal and left exit foramina involvement causing regional spinal canal

stenosis and impingement of left exiting nerve root, the lesion most likely represent metastasis or infection (tuberculous spondylitis, pyogenic spondylitis). He was referred to the medical Department of Hospital Selayang and admitted. Chest x-ray done revealed a suspicious mass involving the right middle and upper lobe (Figure 1).

He was provisionally diagnosed as lung carcinoma with spine metastasis, with a differential diagnosis of pulmonary tuberculosis. Pulmonary tuberculosis work up done revealed AFB smear positive, ESR of 101 and c-reactive protein of 9.54. Patient was started on anti-tuberculosis medications.

One week following treatment with Akurit-4, the patient developed sudden onset left blurring of vision. Ocular examination revealed best corrected visual acuity (BCVA) of 6/9 in the right eye and counting finger of one foot in the left eye. There was left non-axial proptosis of 3mm with exophthalmometer. There was left relative afferent pupillary defect.

Anterior segment examinations of both eyes were normal. The right fundus was normal (Figure 2), however, left fundus revealed total exudative retinal detachment which was bullous involving the superior aspect extending from 9 to 1 o'clock with a shallow detachment temporally involving the macula (Figure 2.1). There were 2 spots of calcification seen inferiorly. Ultrasonography (B scan) of the left eye revealed a choroidal mass with retinal detachment (Figure 3).

Patient was diagnosed as left exudative retinal detachment secondary to probably choroidal metastasis. Patient was referred back to medical with the suspect of malignancy and CT TAP was done. The scan showed a large heterogeneously

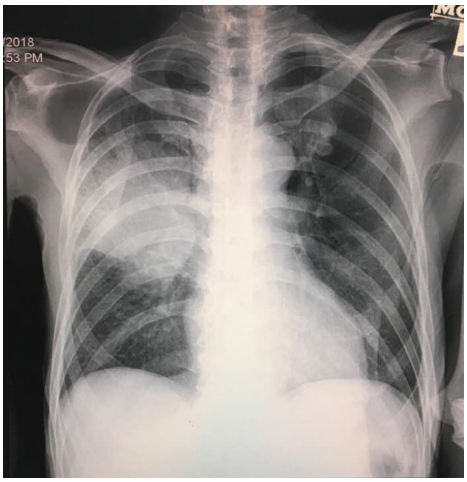

Figure 1: Chest x-ray shows suspicious mass in the right upper and middle lobes.

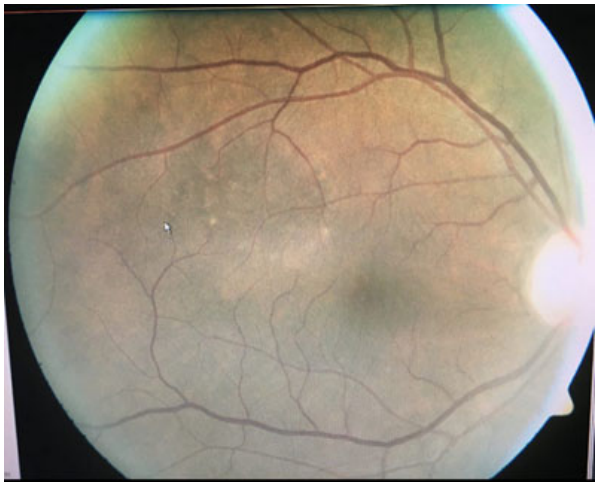

Figure 2: Right fundus photograph.

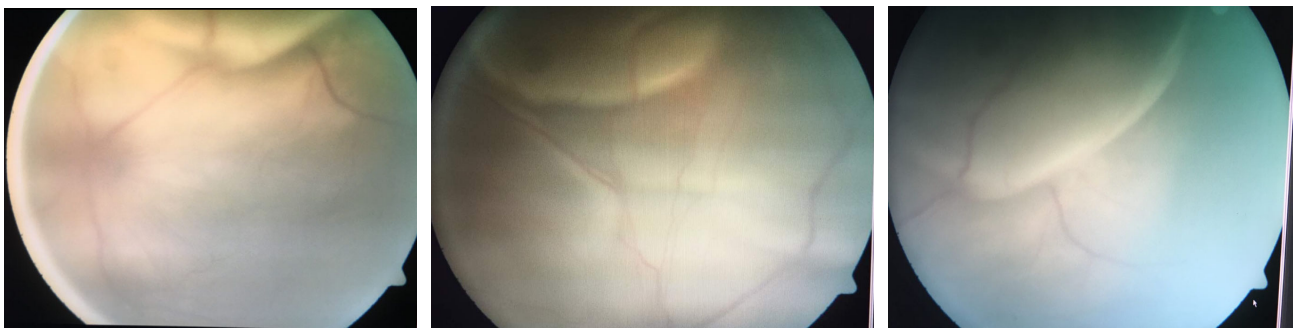

Figure 2.1 : Left fundus photograph shows total exudative retinal detachment which is bullous over the superior quadrant extending from 9-1o'clock with a shallow detachment at the macula and temporally.

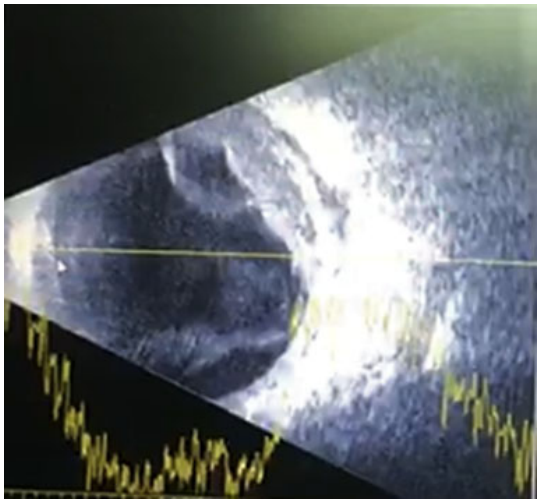

Figure 3: B scan of left eye shows choroidal mass with retinal detachment .

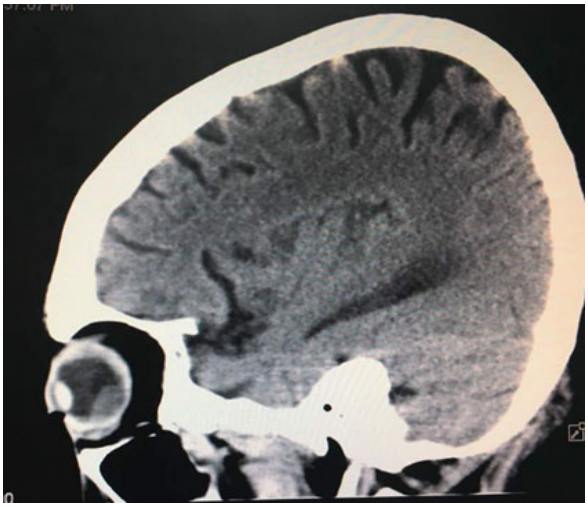

Figure 4: sagittal cross section of CT brain shows choroidal mass in the left eye.

enhancing mass measuring 6.8x7.3x7.1 cm in the upper lobe of the right lung with a regular and spiculated margin with multiple small satellite nodules surrounding it. There was multilevel bone metastases at C5-C6, T9-T10, L3-L5, S1-S2 with soft tissue component causing multilevel spinal canal stenosis and nerve roots impingement. Impression was in keeping with upper lobe right lung mass with nodal, liver and bone metastases. Patient was offered bronchoscopy for biopsy however he refused. Blood investigation revealed hypercalcemia, calcium level of 3.5 and full blood picture showed mild anemia with reticulocyte count of 0.95%.

Patient subsequently developed pneumonia and acute kidney injury secondary to poor oral intake. He was treated with intravenous Rocephine however he deteriorated and succumbed to his illness.

DISCUSSION

The most common intraocular malignant neoplasm in adults is the metastatic carcinoma to the eye [2]. The uveal tract is the most common part of the eye involved by metastases. Within the uvea, the choroid (88%) is the most commonly affected site followed by the iris (9%) and ciliary body (2%) [3]. The reason for this unusual site to be of target for secondary metastases is generally unknown, but it is postulated that its high vascularity may be the reason[3,4]. Metastatic emboli travel through the internal carotid artery, the ophthalmic artery and the posterior ciliary arteries to make their way to the choroid where they can seek a receptive environment for growth. The most frequent origins of choroidal metastasis in decreasing order in women are the breast, the lung, the unknown site, the gastrointestinal tract and the skin melanoma. In males the list is headed by the lung, followed by the unknown location, gastrointestinal tract, the prostate, kidney and skin melanoma [5,6]. The differential diagnosis of choroidal metastasis include choroidal melanoma, choroidal osteoma, choroidal heman-gioma, choroidal neovascularization with disciform scarring, tuberculoma and posterior scleritis [7].

Studies have shown that 63%-72% of patients with a diagnosis of uveal metastasis from lung cancer do not have a known diagnosis of lung cancer at presentation [4].

Visual symptoms may be the first manifestation of systemic metastases. The ocular symptoms that the patient typically presents are blurred vision in 80% of patients, pain in 14%, photopsia in 13%, red eye and floaters in 7% and visual field defects in 3% [7]. In a study by Shields et al, ocular pain was a more common presenting symptom of uveal metastasis from lung cancer compared with all other primary cancers grouped together (14% vs. 7%). It was postulated that this could be due to greater invasiveness, particularly into the sclera and more rapid growth indicated by greater mean thickness of uveal metastasis from lung cancer compared with breast cancer [8,9,10]. Non–small cell carcinoma predominated over small cell carcinoma (84% vs. 16%) [4,8,9].

Clinically, metastatic tumors presented as a creamy yellow appearance (93%) with plateau configuration (67%), with overlying orange-brown pigment (lipofuscin pigment) (7%) and showed multifocality and bilateralism [4,7]. Visual symptoms are caused not only by the mass effect of the tumour, but also by increased subretinal fluid, retinal edema and retinal detachment. Persistent retinal detachment ultimately results in irreversible visual loss that greatly affects the patient's quality of life.

This patient presented at a very late stage. The survival time from diagnosis of uveal metastasis is

between 7-21 months. A number of treatment options are available, including radiotherapy, e.g., external beam, plaque brachytherapy, Gamma Knife, and proton beam, laser therapy, cryotherapy, resection, intravitreal injections and observing for effectiveness of systemic therapy. The choice of treatment varies depending on patient's specific clinical condition. Systemic therapy has been shown to be effective for controlling metastatic tumors of the choroid and is considered to be the preferred treatment option. This treatment is thought to be effective due to the absence of a blood ocular barrier and easy diffusion of systemic medication to the choroid via the fenestrated endothelium of the choriocapillaris.

Regression of the choroidal metastasis with use of systemic chemotherapy alone has been noted. The decision to treat locally has to take into account important considerations such as patient preference, overall health, location and extent of the lesions, and visual symptoms. In patients with choroidal metastasis, the goal of treatment is to improve visual acuity as well as the patient's overall quality of life during the remaining life span [4].

CONCLUSION

Choroidal metastases is the most common intraocular malignancy in the adult population, yet they are not frequently encountered in practice as majority of patients with choroidal metastasis have advanced systemic disease drawing the attention away from the ophthalmic clinical manifestation. A high index of suspicion is essential and a timely referral and review is needed.

REFERENCES

1. Singh N, Kulkarni P, Aggarwal AN, Mittal BR, Gupta N, Behera D, et al. Choroidal Metastasis as a Presenting Manifestation of Lung Cancer: A Report of 3 Cases and Systematic Review of the Literature. Medicine. 2012;91(4):179-94.
2. Sofia Lampaki, Ioannis Kioumis, Georgia P. et al. Lung Cancer and Eye Metastases. Med Hypothesis Discov Innov Ophthalmol. 2014 Summer; 3 (2): 40–44.
3. Christos Asteriou, Dimitrios Konstantinou et al. Blurred vision due to choroidal metastasis as the first manifestation of lung cancer: A case report . World J Surg Oncol. 2010; 8: 2.
4. Sanket U. Shah MD, Arman Mashayekhi MD et al. Uveal Metastasis from Lung Cancer: Clinical Features, Treatment, and Outcome in 194 Patients. American Academy of Ophthalmology. January 2014,Volume 121, Issue 1, Pages 352–357.
5. Abhishek Singh , Parul Singh, Kamal Sahni et al. Non-small cell lung cancer presenting with choroidal metastasis as first sign and showing good response to chemotherapy alone: a case report. J Med Case Reports 2010; 4:185.
6. Samer S. Jamal K. et al. Choroidal metastasis as the sole initial presentation of metastatic lung cancer. Hematology/Oncology and Stem Cell Therapy. Volume 5, Issue 1, January–March 2012, Pages 60-65.
7. Michael Lam, Jason Lee et al. Choroidal metastasis as the presenting feature of a non small cell lung carcinoma with no apparent primary lesion identified by X-ray: A case report. Oncol Lett. 2014 Oct; 8(4): 1886–1888.
8. Iwao Shimomura, Yuji Tada et al. Choroidal Metastasis of Non-Small Cell Lung Cancer That Responded to Gefitinib. Case Reports in Ophthalmological Medicine. Volume 2013, Article ID 21312.
9. Meziani, L., Cassoux N. , Ve Rouic et al. Uveal Metastasis revealing Lung Cancer. J Fr Ophthalmol. 2012; 35: 420-425.
10. Kreusel, K.M., Bechrakis, N.E., Wiegel, T. et al. Incidence and clinical characteristics of symptomatic choroidal metastasis from lung cancer. Acta Ophthalmol. 2008; 86: 515-51.

Case Report

RARE ISOLATED BONY METASTASES TO THE CRANIUM IN ADVANCED COLON CARCINOMA AND THE SCINTIGRAPHY PATTERN SEEN ON BONE SCAN: A CASE REPORT

Noor Azilah Ahmad Tajudin[1], Ahmad Zaid Zanial*[1]

[1]Nuclear Medicine Department, Hospital Kuala Lumpur, Ministry of Health Malaysia
Jalan Pahang, 50586 Kuala Lumpur, Malaysia.

ARTICLE INFO

Corresponding author:
Dr. Ahmad Zaid Zanial

Email address:
ahmadzaidx@gmail.com

Received:
May 2019
Accepted for publication:
June 2019

Keywords:

bone scan
cranium metastases
colorectal carcinoma

ABSTRACT

Although infrequently encountered, skeletal metastases to spine, pelvis and long bones in colorectal cancer have been reported. However, isolated bone metastasis at the cranium is unusual. As for bone scan, it is a sensitive imaging modality commonly used to evaluate bone lesions. Hence, we report a case of advanced colon carcinoma with isolated bone metastases at the cranium to highlight this rare condition and the scintigraphy findings seen on bone scan. A 70 year-old lady with sigmoid colon adenocarcinoma underwent laparoscopic anterior resection in February 2013. Staging computed tomography (CT) scan showed bilateral lung metastasis. She received and completed twelve cycles of chemotherapy in October 2013. Repeat CT scan demonstrated no obvious local recurrence and fairly good response of pulmonary metastases towards chemotherapy. She unfortunately developed painful left posterior scalp swelling in early 2015. A destructive bony lesion with soft tissue component was noted at left posterior parietal bone and smaller lytic lesion seen at right occipital bone on CT scan that were suggestive of metastasis. Bone scan performed in June 2015 to ascertain other bony involvement had revealed features of isolated cranium metastases at left posterior parietal and right occipital regions. No other areas of increased tracer uptake visualised elsewhere especially the vertebrae, pelvis and long bones. Bone metastases to the cranium in advanced colon carcinoma without other skeletal involvement are rare. Bone scan findings of this patient had supported the diagnosis by excluding other sites of metastatic osteoblastic or mixed lytic-sclerotic bone lesions.

INTRODUCTION

Colon and rectal carcinoma or colorectal cancer (CRC) is the third most common cancer worldwide [1]. CRC has significant mortality risk. It was estimated that 56% of patients die from their cancer [1]. In Malaysia, CRC is one of the ten most frequent cancers encountered. Latest local data demonstrated that overall incidence rate was 21.23 cases/100000 and mortality rate of 9.79 cases/100000 based on the previous National Cancer Registry [2].

Approximately 20% of patients with CRC already have metastases at diagnosis [1]. The commonest sites for metastases are liver and lungs. Hence, staging of the disease is an important aspect in CRC management. Although infrequently encountered, skeletal metastases to the spine, pelvis and long bones have been reported [3]. Similarly, the cranium or skull is an unusual site for bone metastasis in CRC [4,5].

Bone scan or scintigraphy performed using phosphate analogues labelled with isotope Technetium-99m has good skeletal localisation in area with osteogenic activity or osteoblastic process. It is commonly done with standard head-to-toe image acquisition. Bone scan is an established method for demonstrating skeletal diseases and being associated with high sensitivity but low specificity [6]. It enables whole-body scanning at relatively low radiation and low cost [7].

Bone scan has been recognised as an important oncological investigation and widely used to evaluate skeletal metastases mainly in prostate, breast and lung cancers. Although less commonly performed in CRC patients, it has been noted that several studies have utilised bone scan to complement evaluation of bone metastasis [3]. Hence, we report a case of isolated bony metastases to the cranium in advanced colon carcinoma to highlight this rare condition and its scintigraphy findings seen on bone scan.

CASE REPORT

A 70 year-old lady with sigmoid colon adenocarcinoma had undergone laparoscopic anterior resection in February 2013. Staging computed tomography (CT) scan showed bilateral lung metastases. Postoperatively, she received and completed twelve cycles of 5-fluorouracil-leucovorin based adjuvant chemotherapy in October 2013. Subsequently, a repeat CT scan demonstrated no obvious local recurrence and fairly good response of pulmonary metastases towards the chemotherapy.

She unfortunately developed painful left posterior scalp swelling in early 2015 and was later subjected to further investigations. A destructive bony lesion with soft tissue component was noted at left posterior parietal bone and smaller lytic lesion seen at right occipital region of the skull as seen on CT scan, suggestive of bone metastases. However, there was no demonstrable CT evidence of intra-parenchymal brain lesions seen.

A whole-body bone scan was performed in June 2015 to ascertain other bony involvement. It revealed abnormal increased tracer uptake at the right occipital region and another lesion of circumferential tracer uptake surrounding a photon-deficient area at the left posterior parietal region as shown in Figure 1. Supplementary imaging using single photon emission computerised tomography with computed tomography (SPECT-CT) of the skull was also done as shown in Figures 2 and 3.

No other areas of increased tracer uptake or significant photon-deficient lesions visualised elsewhere especially in the vertebrae, pelvis and long bones. Hence, the bone scan findings were suggestive of isolated cranium metastases. In view of the localised bone metastases, she then underwent palliative radiotherapy to the skull. However, she finally succumbed to her illness approximately six months later in December 2015.

DISCUSSION

Metastatic spread from colonic cancer is initially by the lymphatics followed by haematogenous route [8]. From colon and proximal rectum, blood is drained through portal system to the liver and via the heart to the lungs. On the other hand, blood drainage from distal rectum surpasses the liver and first encounter the lungs [1]. Hence, bone metastases rarely occur in the absence of visceral metastatic disease [3].

Nozue M, et al. (2002) found that only 1.3% of resected primary CRC cases in a previous study involving 928 patients had bone metastasis [9]. Nevertheless, all of these cases with bone metastasis were highly advanced stage at the time of

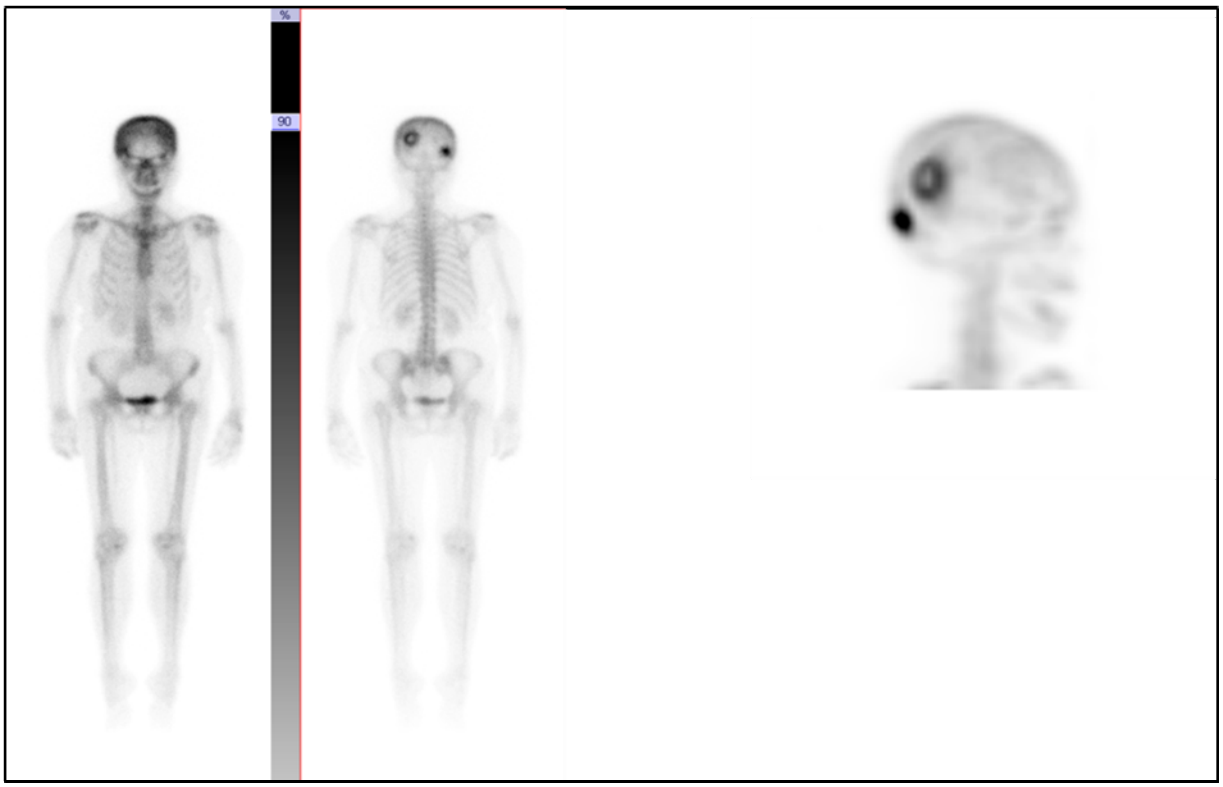

Figure 1: Whole-body bone scan and spot view of the skull images show abnormal increased tracer uptake at the right occipital region and another lesion of circumferential tracer uptake surrounding a photon-deficient area at the left posterior parietal region.

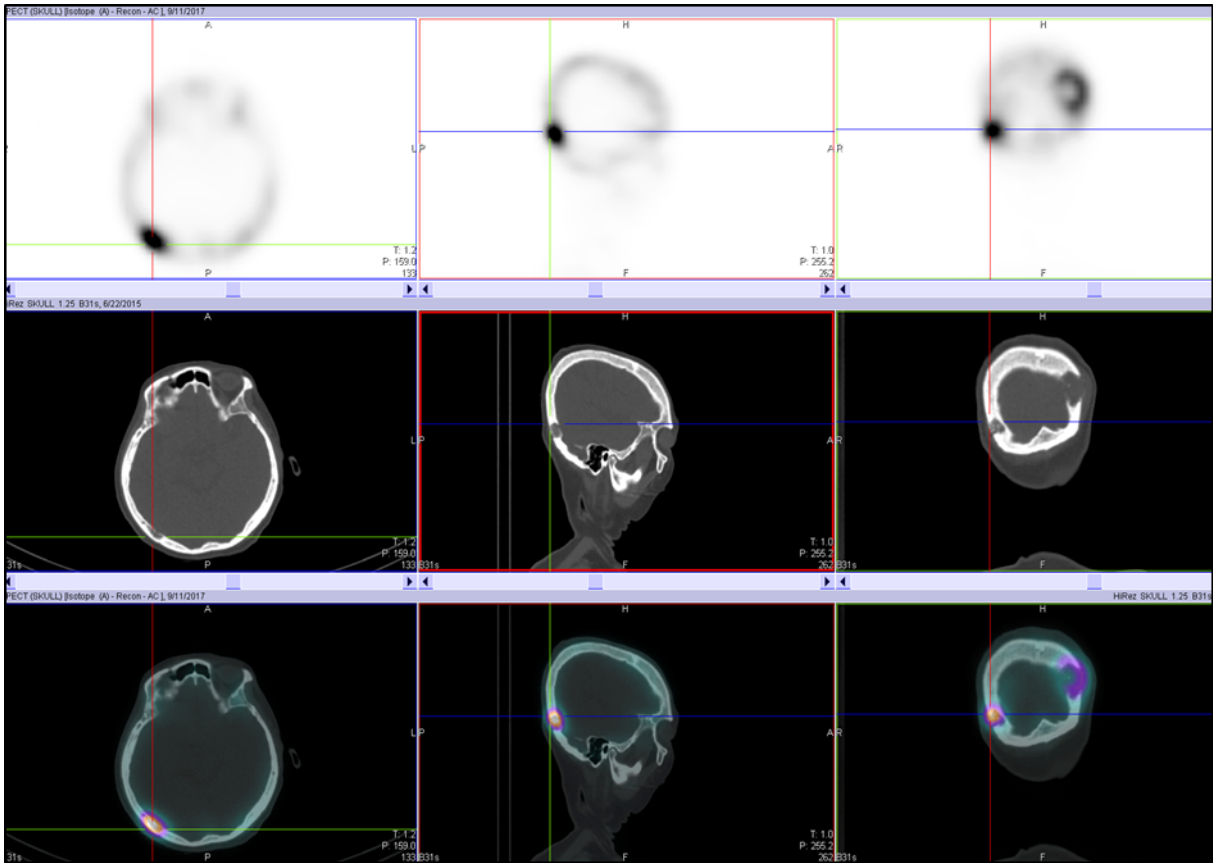

Figure 2: Hybrid SPECT-CT of skull (bone-window) images show abnormal increased tracer uptake at the cranium corresponding to destructive lytic bone lesions with slightly sclerotic edges.

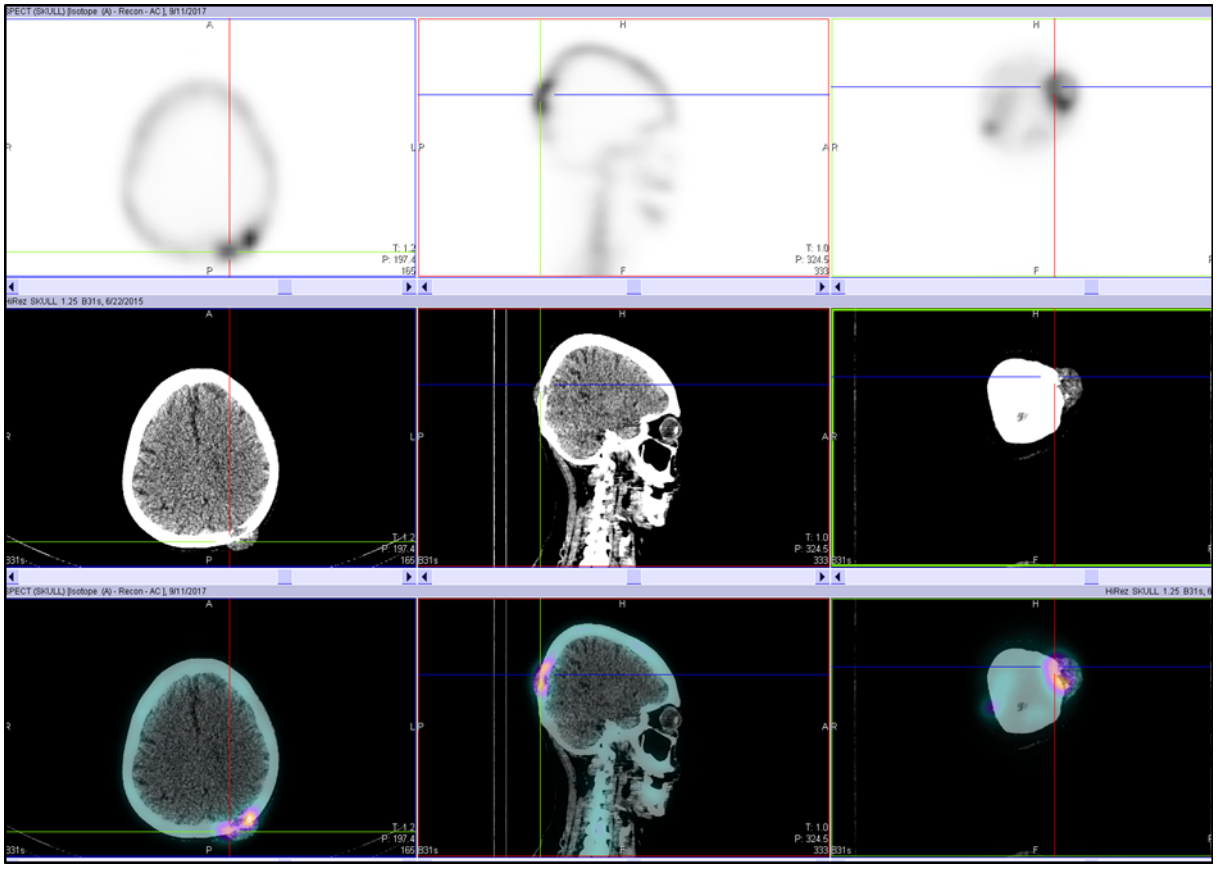

Figure 3: Hybrid SPECT-CT of skull (soft tissue-window) images demonstrate a destructive lesion with soft tissue component at left posterior parietal region no obvious intracranial extension or involvement of the adjacent brain parenchyma.

diagnosis. At the onset of bone metastasis, nine cases also had other metastatic sites compared with only three cases with bone metastasis alone [9].

In terms of skeletal metastasis in CRC, the commonly involved bones were the vertebrae (65%) followed by pelvis-hip (34%) and long bones (26%) [10]. The postulated factors behind this metastatic pattern are due to the para-vertebral valveless venous plexus of Batson, arterial spread to appendicular skeleton and breakage of lymphatic system especially if these lymphatics do not belong to the portal system [3].

Osteolytic lesions were found to be more prevalent (81%) compared to mixed lesions (13%) and osteoblastic lesions (6%) in CRC patients with bone metastases [10]. Osteoblastic reparative activity in response to tumour osteolytic process will lead to increased tracer accumulation seen on bone scan and the scintigraphy pattern of multiple randomly distributed foci of tracer uptake of varying size, shape and intensity is highly suggestive of bone metastases [11].

A patient with diffuse mixed sclerotic-lytic bone lesions seen on CT scan was reported to have widespread skeletal metastases including the skull as depicted on bone scintigraphy in a case series involving few CRC cases presenting with back pain [3]. Nonetheless, metastatic disease occasionally manifests as a solitary abnormality usually in the spine as well as an area of decreased rather than increased tracer activity [11].

Osteolytic metastasis giving rise to photon-deficient lesions at axial skeleton on bone scan has been documented previously [12]. Our patient showed abnormal scintigraphy pattern of increased tracer uptake at right occipital region and another lesion of circumferential tracer uptake surrounding a photon-deficient area at left posterior parietal region. Otherwise, her whole-body scintigraphy revealed no other significant abnormal findings elsewhere in the skeletal system and thus indicating isolated cranium metastases.

Cranium metastases are considered rare entity and could present either at diagnosis or as an initial symptom of recurrence with the absence of visceral metastasis and vertebral or other skeletal involvement [4,5,13]. Rodrigues J, et al. (2012) reported a 62 year-old lady had presented with left forehead swelling without any history of trauma or neurological deficit. Her investigations confirmed a metastatic hepatic flexure adenocarcinoma with no liver or lung metastasis [13].

In another case report, a 65 year-old lady with history of resected colorectal adenocarcinoma has been disease-free for five years before presenting again with a progressively increasing in size of right fronto-parietal destructive bony metastasis [4]. Whereas, Kacan T, et al. (2014) has reported a 44 year-old man with rectal adenocarcinoma post-surgery and adjuvant chemotherapy whom developed rapidly growing right parietal bone metastasis after being in remission for three years [5].

Survival after the onset of bone metastasis in CRC was demonstrated to be very poor with median survival of five months and a survival rate of 20% at one year [9]. Furthermore, in a large study comprising 264 patients with CRC involving bones, the median overall survival after diagnosis of bone metastasis was noted around seven months (95% CI 5.75 – 8.70 months) with higher number of lesions and osteolytic type being associated with shorter median survival ($p<0.05$) [10]. Both studies included bone scan as part of the staging investigations.

Although not performed for this patient, another important molecular imaging that can be done was the flurodeoxyglucose (FDG) positron emission tomography with computed tomography (PET-CT). Imaging with FDG has been accepted and demonstrated as an effective method in the assessment of metastasis, recurrence, patient selection for surgery and treatment response evaluation that could lead to changes in CRC management. FDG PET-CT is both sensitive and specific in diagnosing bone metastasis with excellent positive predictive value [14].

CONCLUSION

Bone metastases in CRC are associated with poor prognosis. Bone scan could be a useful investigation tool for advanced CRC as demonstrated in this case report and may affect management decisions. Bone metastases to the cranium in advanced colon carcinoma without other skeletal involvement are rare. Bone scan findings of the patient in this case report had supported the diagnosis by excluding other sites of osteoblastic or mixed lytic-sclerotic metastatic bone lesions.

ETHICS

This case report has been registered with the National Medical Research Register, Ministry of Health Malaysia (NMRR-19-907-48053) and received the permission from the Head of Nuclear Medicine Department, Hospital Kuala Lumpur. Efforts have been taken to ensure confidentiality of our patient. The authors declare no conflict of interests and did not receive any fund or grant for this case report publication.

ACKNOWLEDGEMENT

We would like to thank the Director General of Health Malaysia for his permission to publish this article. We also like to acknowledge our dedicated colleagues and staff at the Nuclear Medicine Department, Hospital Kuala Lumpur for their continuous support, encouragement and kind assistance.

REFERENCES

1. Riihimaki M, et al. (2016). Patterns of metastasis in colon and rectal cancer. Scientific Reports; 6: 29765. doi:10.1038/srep29765.
2. Hassan WRA, et al. (2016). Incidence and mortality rates of colorectal cancer in Malaysia. Epidemiol Health; 38: e2016007.
3. Assi R, et al. (2015). Metastatic colorectal cancer presenting with bone marrow metastasis; a case series and review of literature. J Gastrointest Oncol.; 7(2): 284-297.
4. Firat C, et al. (2012). Atypical presentation of skull metastasis from rectal adenocarcinoma as an initial symptom of recurrence. Case Reports in Medicine; 794354. doi:10.1155/2012/794354.
5. Kacan T, et al. (2014). Parietal bone metastasis of rectal adenocarcinoma as an initial diagnosis of recurrence: Case report. SAJ Case Rep.; 1: 101. doi:10.18875/2375-7043.1.101.
6. Hin S.F., et al. (2002). Functional imaging and the orthopaedic surgeon. Journal of Bone and Joint Surgery; 84: 3: 315-321.
7. Ilaslan H., et al. (2010). Clinical presentation and imaging of bone and soft-tissue sarcomas. Cleveland Clinic Journal of Medicine; 77: 1.
8. Attili VSS, et al. (2006). Unusual metastasis in colorectal cancer. Indian Journal of Cancer; 43 (2): 93-95.
9. Nozue M, et al. (2002). Treatment and prognosis in colorectal cancer patients with bone metastasis. Oncol Rep.; 9(1): 109-112.
10. Santini D, et al. (2012). Natural history of bone metastasis in colorectal cancer: final results of a large Italian bone metastases study. Annals of Oncology; 23: 2072-2077.
11. Love C, et al. (2003). Radionuclide bone imaging: An illustrative review. RadioGraphics; 23: 341-358.
12. Aydın M, et al. (2005). Photon-deficient bone metastases secondary to pleural malignant mesothelioma. Turk J Nuclear Med.; 14: 65-67.
13. Rodrigues J, et al. (2012). A Rare Case of Colon Cancer with Metastases to the Bone with Review of the Literature. The Internet Journal of Oncology; 8(2).
14. Cinar A, et al. (2013). Restaging of colorectal cancer and PET/CT. Ulusal Cer Derg.; 29: 76-80.

Original Article

ANALYTICAL STUDY OF KETAMINE FROM DIFFERENT AQUEOUS MEDIUM FOR FORENSIC DETERMINATION

Norzita Mohamed*[1], Chang Kah Haw [2], Ahmad Fahmi Lim Abdullah[2]

[1]Department of Forensic Medicine , Hospital Sultanah Nur Zahirah, 20400 Kuala Terengganu, Terengganu, Malaysia.
[2]School of Health Sciences, Universiti Sains Malaysia, 16150 Kubang Kerian, Kelantan, Malaysia.

ARTICLE INFO

Corresponding author:
Norzita Mohamed

Email address:
gieyta@yahoo.com

Received:
April 2019
Accepted for publication:
June 2019

Keywords:
Ketamine analysis
method development
GC-FID
sample recovery

ABSTRACT

Ketamine is widely used as a drug of abuse. A study was conducted to develop a simple and rapid gas chromatography- flame ionization detector (GC-FID) method for the analytical study of ketamine from different aqueous medium sample. The developed method was selective as chromatogram showed no interferences and overlapped peak eluted at the retention time where ketamine eluted. A linear relationship of peak area ratio versus concentration (µg/mL) was obtained in the range of ketamine concentration 31.25 µg/mL - 500.00 µg/mL with r^2 = 0.994. The precision and accuracy of the method were within the acceptable limits. Various sample recovery rates were established with Coca-cola drink showing the highest recovery among the drinks tested. The urine sample spiked with ketamine also gave reasonable recovery value, though higher recovery rate from urine might be obtained through other extraction strategy.

INTRODUCTION

Ketamine is *N*-methyl-D-aspartate (NMDA) receptor - antagonist and chemically known as 2-(2-chlorophenyl)-2-(methylamino)-cyclohexan-1-one, with empirical formula $C_{13}H_{16}ClNO$ and with molecular weight of 237.73 g/mol [1]. Physically, ketamine can appear as free base or hydrochloride salt. Ketamine hydrochloride salt is a white crystalline powder and is easily dissolved in water forming a free base [1]. Its structure is shown in Figure 1**.**

In response to its anaesthesiology properties, ketamine was initially developed in early 1960s for the clinical purposes especially during surgeries [2, 3]. However, ketamine was later reported to be abused as a 'date rape' drug and also a drug-facilitated sexual abuse (DFSA) [4]. Ketamine was namely as such due to the reason that it is frequently used by the assailants to commit sexual assaults and other criminal offences [5]. Ketamine is colourless, odourless and tasteless, therefore it can be easily added and dissolved in drinks without being easily noticed by the victim [6, 7].

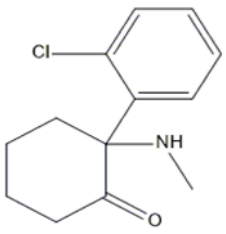

Figure 1: Chemical structure of ketamine

In Malaysia, ketamine is categorised as a Schedule I and placed under Amphetamine-Type Stimulant (ATS) drug in the Dangerous Drug Act (1952) [8]. This means that unauthorised possession of it is illegal. A statistic from Royal Malaysia Police reported by Singh, Chawarski [9] indicated that, the number of ketamine users have considerably increased from year 2006 to 2012. The drugs were sold in the original form or in the latest scenario, added into energy drink, soft drink, flavoured drink and alcoholic drinks [10].

The purpose of the present study was to develop a validated method for the recovery of ketamine in various aqueous medium for the forensic determination. The preliminary study involved the

development of method followed by optimisation, validation and recovery study on drinks and urine samples. The validation of the method was assessed by performing the selectivity, linearity, precision (reproducibility and repeatability) and accuracy study, limit of detection (LOD) and limit of quantification (LOQ) and recovery study using GC-FID method [11-14]. The recovery study was performed on five selected drink samples; Coca-Cola, Red bull, Livita, 100 plus, Nescafe® original and one biological sample, pooled human urine.

MATERIALS AND METHODS

Reagents and chemicals

Analytical grade dichloromethane (DCM) was purchased from Merck KGaA, Germany.Standards, including ketamine hydrochloride (98%), methamphetamine,*3,4-methylenedioxy-methamphetamine* (MDMA) and caffeine were supplied by Chemistry Department of Malaysia.Internal standard (IS) n-Octadecane (99.6%) was sourced from Dr Ehrenstorfer GmbH (Augsburg, Germany).

Instrumentation

GC-FID

The analysis was performed using Agilent 7890A gas chromatograph coupled with flame ionization detector (FID). The liquid samples were injected into GC-FID by means of auto sampler. A volume of 1 µL of sample was introduced into the injection port. The GC automation and data analysis on the system was completed via Chemstation software (revision B.04.02) (Agilent Technologies, Santa Clara, CA). The GC-FID has a split-splitless inlet system operated in the splitless mode and the injector temperature was set to 250^{o}C, pressure at 7.3267 psi, septum purge flow 3 mL/min and purge flow to split vent is 40 mL/min at 0.75 min.

The chromatographic separation was accomplished on an Agilent J & W 19091J-413 HP5 fused-silica capillary column (30m length x 0.320 mm i.d. x 0.25 µm film thickness) purchased from Agilent Technologies. The purified nitrogen gas with 99.999% purity was used as the carrier gas at 1.0 mL/min at a constant flow rate mode. The oven temperature program was set up as follows: first held at 150^{o}C/ min for 1 min, ramp at 10^{o}C/min until the temperature reached 220^{o}C and finally ramping at 90^{o}C/min until 290^{o}C/min, held for 3 minutes. The total analysis time was 11.778 min. The resulting peak in the chromatogram obtained were identified and analysed.

GC-MS

Agilent Technologies GC equipped with an Agilent5977A mass selective detector (MSD), an Agilent 7693 autosampler and an Agilent Mass Hunter for data acquisition. The GC-MS had a split-splitless inlet system operated in the splitless mode. The analytical column was an Agilent DB-5MS silica capillary column (30 m length x 0.250 mm i.d. x 0.25 µm film thickness) using helium gas (99.999% purity) as the carrier gas at 1.0 mL/min. The mass spectrometer operates at a full scan mode. With the identical column and chromatographic condition settings, the total ion chromatographic (TIC) obtained was recorded and compared.

Sample collection

Regular Coca-cola, Red Bull, Livita, 100 Plus Original Isotonic and Nescafe® original drinks were purchased from local groceries and pooled human urine was collected from non-ketamine user volunteers of two males and two females The ethics for the human biological sample was approved by Human Research Ethics Committee of USM (HREC) coded USM/JEPeM/16050194.

Preparation of the standard solutions and validation samples

Ketamine hydrochloride stock solution at concentration 1000 µg/mL was prepared by weighing 10.0 mg of ketamine hydrochloride powder accurately using an analytical balance and then transferred into a 10 mL volumetric flask. DCM was added into the volumetric flask up to the mark and homogenised by gently inverting the flask to ensure that the ketamine white powder was completely dissolved in the solvent.

Preparation of Internal Standard (IS) Stock Solution

n-Octadecane (C-18) at concentration 100 µg/mL was used as an internal standard (IS) stock solution. Ten miligrams of C-18 was accurately weighted using analytical balance and dissolved in 100 mL of DCM in a 100 mL volumetric flask. The IS solution was homogenised by gently inverting the volumetric flask.

Preparation of Working Standard Solutions

A working standards were prepared from the 1000 µg/mL stock solutions with a serial dilution techniques. These working standards were prepared in seven serial dilutions with a total volume of 10 mL each and in decreasing concentration ranged from 500 µg/mL - 7.81 µg/mL.

For the preparation of working standard at concentration 500 µg/mL, 5 mL of stock solution was aliquoted into a 10 mL volumetric flask. The flask containing 5 mL of stock solution was topped up with 5 mL of DCM to make up a final volume of 10 mL and homogenized. For the preparation of working standard at second concentration level i.e., 250 µg/mL, 5 mL of the first working solution at 500 µg/mL was transferred into another 10 mL volumetric flask and topped up with DCM to the mark. The same dilution procedure was applied for the next concentration of working standard. Table 1 summarises the measurements used to prepare the working standards.

Table 1: Preparation of the working standards at seven concentrations.

Working standard	Concentration of working standard (µg/mL)	Volume of working std at previous concentration level (mL)	Volume of DCM (mL)	Total volume of working standard (mL)
Working std. 1	500	5	5	10
Working std. 2	250	5	5	10
Working std. 3	125	5	5	10
Working std. 4	62.5	5	5	10
Working std. 5	31.25	5	5	10
Working std. 6	15.63	5	5	10
Working std. 7	7.81	5	5	10

Preparation of 1.0 M Sodium Hydroxide (NaOH)
Sodium hydroxide (NaOH) was used during sample extraction to achieve optimum pH for ketamine recovery study. NaOH (1.0 M) was prepared by dissolving 4 g of NaOH pallette into 100 mL of deionised water in a 100 mL volumetric flask. The palette was stirred and then transferred into a bottle, capped, labelled and kept at room temperature.

Optimization of the extraction method
The extraction procedure was optimised as a two-steps liquid-liquid extraction (LLE) technique using DCM as an extraction solvent. A sample volume of 10 mL was aliquoted into an assembly of glass tubes and the pH were adjusted to alkaline condition ranging from pH 10-13 by the addition of NaOH solution. Two mililitres of DCM was added into the samples and shaken for 10 minutes. The samples were then briefly vortexed and centrifuged at 5000 rpm for 5 minutes. The lower layer of the mixture containing the analyte of interest was pipetted out and transferred into a new tube. After that, the second extraction step was carried out by the addition of 2 mL DCM into the sample. The process of extraction was repeated. The lower organic layer of the second extraction was combined into the same tubes and then evaporated. When the solvents reached near dryness, 500 µL of the solvents were aliquoted into the chromatographic vial and reconstituted with 500 µL of IS stock solution. The vial is then place in the GC sample rack and run by auto injection programme set in the GC-FID.

Validation
Selectivity, linearity, limit of detection (LOD), limit of quantification (LOQ), precision and accuracy as well as sample recovery were investigated for validation studies. Method selectivity study was determined by spiking five known standards; methamphetamine, 3,4-methylenedioxymethamphetamine (MDMA), caffeine, ketamine standard and internal standard n-Octadecane (C-18) in DCM and analysed by GC-FID for peak separation studies. Separated peak was then confirmed by injecting the same sample in GC-MS where the retention time and identity of the compounds were established by mass spectral analysis. For LOD and LOQ, a range of ketamine working standards as prepared in Table 1 were analysed at highest concentration until to the lowest concentration that were no longer detectable by the GC-FID. The LOQ was calculated as three times of LOD value.

The linearity study was established by preparing a standard solution at five concentration levels ranged from 500 µg/mL to 31.25 µg/mL. A total of six injections of every standards concentration were performed using GC-FID. The results obtained were further calculated for the peak area ratio of the standards using Equation 1.

$$\text{Peak area ratio} = \frac{\text{peak area of ketamine standard}}{\text{peak area of IS}}$$

...Equation 1

A calibration curve was plotted using Microsoft Excel®. A linear regression equation, the intercept and the r-squared (r^2) were determined. The precision study (repeatability and reproducibility) was implemented by analysing ketamine standards at three nominal concentration levels; low (50 µg/mL), medium (200 µg/mL) and high (400 µg/mL). Seven injections of standards were run at each concentration level. For repeatability, the measurement for all standards concentration were taken within the same day using the same instrument and within the same period meanwhile, for reproducibility, the same standards concentration levels were analysed at three injections on three consecutive days. The precision was expressed as % RSD.

The percentage of accuracy were determined at three replicates for each concentration level and analysed at three consecutive days. For sample recovery study, the spiked standard samples were prepared at two different concentration levels; 500 µg/mL and 100 µg/mL with three replicate samples for each spiked sample. After prepared, these two concentration levels of spiked samples were analysed for the target analyte. The results obtained were tabulated in tables and the recovery was reported in percentage.

RESULTS

Selectivity study

The peak of a known standard must be well separated and specifically identified in the chromatogram. Thus, in this analytical method development study, the selectivity testing was conducted to ensure that a peak of a known standard was not interfered with other analytes potentially present together. Figure 2 below shows the chromatograms of a separation of mixed standard containing methamphetamine, MDMA, IS, caffeine and ketamine standard dissolved in DCM analysed using GC -FID.

Limit of detection (LOD) & Limit of Quantification (LOQ)

From this experimental study, it was determined that the LOD obtained was 7.82 µg/mL. The calculated LOQ was determined as 23.46 µg/ mL.

Intra-day and inter-day precision

Intra-day and inter-day precision were recorded as in Table 2 and Table 3.

Recovery study

The samples chosen for recovery study consists of five types of beverages and one type of biological sample namely Coca-Cola, Livita, Red Bull, Nescafe® original and 100 plus isotonic drink and pooled human urine. The results of recovery study for these samples as tabulated in Table 4.

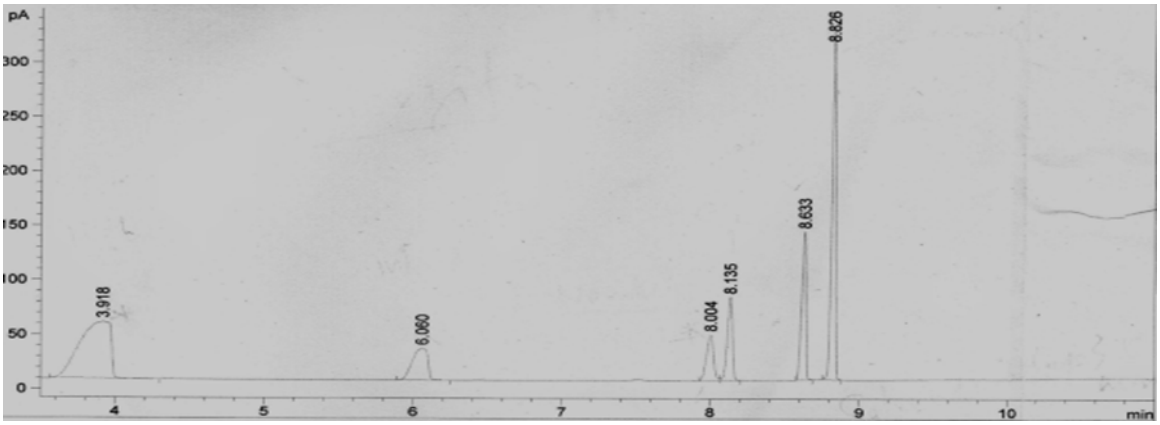

Figure 2: The chromatogram of a known standards spiked in DCM analysed using GC-FID.

Table 2: Intra-day precision study and accuracy of ketamine standard

Level (µg/mL)	Mean ± SD		RSD (%)
50	47.96 ± 1.20		2.51
200	188.97 ± 2.22		1.17
400	383.19 ± 2.30		0.60

Table 3: Inter-day precision and accuracy study of ketamine standard

Level (µg/mL)	Mean ± SD	Accuracy (%)	RSD (%)
50	53.97 ± 0.43	-7.94	1.45
200	189.33 ± 2.85	5.33	1.51
400	408.95 ± 4.13	-2.24	1.01

Table 4: Recovery value of a spiked standards in multi medium samples.

No.	Sample	Recovery(%) ± SD, (n=3)	
		Low concentration of spiked standard (100 µg/mL)	High concentration of spiked standard (500 µg/mL)
1	Coca-cola	80.35 ± 3.83	80.40 ± 10.51
2	Red Bull	72.73 ± 8.81	65.22 ± 11.43
3	Livita	65.67 ± 4.68	66.17 ± 4.66
4	100 Plus	62.15 ± 7.92	72.53 ± 6.84
5	Urine	26.33 ± 0.41	12.52 + 3.52
6	Nescafe® (original)	Unable to extract	Unable to extract

DISCUSSION

The selective properties of one method was tested and the peak of a known standard must be well isolated and specifically identified in the chromatogram. As in Figure 3.1, the resulting peak on the chromatogram for known standards spiked in DCM showed good peak separation. It is clearly indicated that all eluted peaks neither interfere nor overlapped with each other indicating good compound separation under the experimental parameter used. Consequently, the method was specific and selective enough for the determination of analyte of interest in the sample. GC-MS has proved to be able to provide an identification of a compound of every peak discernable on the chromatogram, but varied slightly and shifted in the retention time as may have occurred where there is slight change in the instrument conditions. Using the mass spectrum, all the compounds in the mixed samples were identified, based on the destructive mass spectral features as well as the mass spectra library match.

The GC-FID method was still able to detect the ketamine standard concentration at 7.82 µg/mL but this was very close to the noise level and however could still be confidently distinguished from the adjacent peaks. Therefore from this experimental study, the LOD was determined to be 7.82 µg/mL, meanwhile the calculated LOQ was determined as 23.46 µg/ mL. The calculated LOQ was obtained as the LOD 7.82 µg/ mL multiplied by three given the result of 23.46 µg/ mL

A linear regression equation and correlation coefficient, r-squared value was obtained from the development of a calibration curve. The linear regression equation obtained from the calibration curve was y = 0.0057x - 0.1103. The high r^2 obtained (>0.99) indicates that the data fits in a straight line and the calibration curve is good for response in a linear manner in the range of concentration 31.25 µg/ mL to 500 µg/mL.

Precision is a measure of the dispersion or closeness of results when an analytical procedure is repeated on one sample. Precision reflects the random error which frequently happens in analytical method. There are two common sets of precision study so-called repeatability (intra-day precision) and reproducibility (inter-day precision). Referring to table 3.1 and 3.2, the %RSD for intra-day precision study ranged from 0.60% to 2.51%, whereas for inter-day precision the %RSD ranged from 1.01% - 1.51%.

Among the drinks, Coca-cola drink gave the highest recovery of about 80% at two different concentrations indicating that the matrix effect from Coca-cola drink is minimal. In Red Bull and Livita drinks, the recovery at low concentration was more than 65% while Red Bull suffered from slightly lower recovery for high concentration spiked samples and this reversed from 100 Plus drink. The Nescafe® original drink, did not give any response on GC-FID indicating severe matrix effect that had interfere the sample recovery using the experimental parameters. Urine sample did not give high recovery percentage due to biological sample matrix effect, to have given only about 10% to 30% recovery.

CONCLUSION

This study applied a direct approach for the analytical study of ketamine from different aqueous medium. Drink samples has been chosen due to an increasing trend of 'club drugs' or 'date rape' drugs spiked in beverages especially during special occasions like rave parties, concerts or dance clubs. This analytical study covered an analytical method development, method optimisation and method validation. When compared to UNODC guidelines, all the validation parameters were within the acceptable limits with the exception of recovery value of ketamine in urine.

One of the more significant findings emerging from

this study is that the optimised chromatographic condition was suitable for simultaneous determination of many analytes. Without sample derivatisation, the peak of analytes of interest were still able to be retrieved. Overall, this study strengthens the idea that with direct and simple spiking method with the exception of sample hydrolysis and derivatisation, the recoveries in selected drinks samples and in urine were well performed. It is important to note that a direct recovery from drink samples provide a simple, rapid and reproducible result of analysis in forensic laboratories which routinely receive samples for analysis.

In brief, this is the first time that ketamine has been used to explore in a selected drinks in Malaysia. Hence this would be part of the exploratory study for the recovery of ketamine in such drinks. Despite its exploratory scheme, this study offers some insight into the investigation whether ketamine can be used as a surrogate compound for further drug of abuse analysis.

ACKNOWLEDGEMENT

The author would like to thank to Dr Ahmad Fahmi Lim Abdullah and Dr Chang Kah Haw whom consistently give a guidance during the planning and development in this study. Thank you also to everyone who give the support through this entire -study.

REFERENCES

1. WHO, *Ketamine international non-proprietary name (INN) : update review report.* World Health Organization, 2015. 37: p. 1-46.
2. Favretto, D., et al., *Determination of ketamine and norketamine in hair by micropulverized extraction and liquid chromatography-high resolution mass spectrometry.* Forensic Science International, 2013. 226: p. 88-93.
3. Salomone, A., et al., *Cut-off proposal for the detection of ketamine in hair.* Forensic Science International, 2015. 248: p. 119-123.
4. Norlida , H., R.A. Anderson, and P.A. Cormack, *Analysis of ketamine and norketamine in hair samples using molecularly imprinted solid-phase extraction (MISPE) and liquid chromatography-tandem mass spectrometry (LC-MS/MS).* Analytical and Bioanalytical Chemistry, 2010. 396(7): p. 2449-2459.
5. Anilanmert, B., et al., *Simultaneous analysis method for GHB, ketamine, norketamine, phenobarbital, thiopental, zolpidem, zopiclone and phenytoin in urine using C18 poroshell column.* Journal of Chromatography B, 2016. 1022: p. 230-241.
6. LeBeau, M., et al., *Recommendations for toxicological investigations of drug-facilitated sexual assaults.* Journal of Forensic Sciences, 1999. 44 (1): p. 227-230.
7. Dodich, C. and M. Siedlarz, *Date rape drugs.* International Journal of Child and Adolescent Health, 2014. 7(4): p. 355-368.
8. DDA 1952, *Act 234.* Dangerous Drug Act 1952 (Amendment 2003), 2003: p. 1-55.
9. Singh, D., et al., *Substance abuse and the HIV situation in malaysia.* Journal of Food and Drug Analysis, 2013. 21(4): p. 46-51.
10. Mohamad Azim, F.A.A. *Edar dadah guna botol minuman*. 2015 15 November 2016]; Available from: http://www.hmetro.com.my/node/67980.
11. Green, M.J., *A practical guide to analytical method validation.* American Chemical Society, 1996: p. 305-309.
12. FDA, *Analytical procedures and methods validation for drugs and biologics*, in *Guidance for Industry*2015, Food and Drug Administration Agency: United States. p. 1-15.
13. UNODC, *Guidance for the Validation of Analytical Methodology and Calibration of Equipment used for Testing of Illicit Drugs in Seized Materials and Biological Specimens*, in *United Nations Office on Drugs and Crime*, L.a.S. Section, Editor 2009, United Nations Publication: United Nations, New York.
14. MOH, *Guidelines for testing drugs of abuse in urine*, M.o.H. Malaysia, Editor 2002, Department of Medical Development.

Original Article

MOLECULAR IDENTIFICATION OF BACTERIAL COMMUNITIES FROM VEGETABLES SAMPLES AS REVEALED BY DNA SEQUENCING OF UNIVERSAL PRIMER 16S rRNA GENE.

Nur Syifaa Hanis Ghazali*[1], Nur Haslindawaty Abd Rashid[1]

[1]School of Health Sciences, Universiti Sains Malaysia, 16150 Kubang Kerian, Kelantan, Malaysia.

ARTICLE INFO

Corresponding author:
Nur Syifaa Hanis Ghazali

Email address:
syifaahanis.ghazali@yahoo.com

Received:
May 2019
Accepted for publication:
June 2019

Keywords:

identification of bacteria
16S rRNA gene
PCR optimization
Basic Local Alignment Search Tools (BLAST)

ABSTRACT

Vegetables are parts of the healthy diet to the individuals. Microbes are introduced to the fresh produces starting from the pre-harvesting, post harvesting and even until end to the consumer. The aim of this study is to identify the bacterial community presence on vegetables sample through DNA sequencing of mitochondrial 16S rRNA gene. In this study, 16 types of vegetables, namely chinese broccoli (S1), water spinach (S2), chinese flowering cabbage (S3), spinach (S4), eggplant (S5), sweet potato (S6), tomato (S7), long bean (S8), chili (S9), scallion (S10), capsicum (S11), cauliflower (S12), pak choy/bok choy (S13), french bean (S14), coriander (S15) and carrot (S16) were selected for PCR amplification using universal primer 16S rRNA gene. The result shows the newly designed universal primer was successfully amplified 460 bp partial sequence of 16S rRNA gene. The bacteria community such as Cyanobacterium sp., Sphingomonadales sp, Bacillales bacterium, Actinobacterium, Deinococcus sp., Trichodesmium and Carnobacterium sp. were successfully identified in this study, suggesting that the identification of bacteria can be performed directly from samples without requirement of bacteria culture.

INTRODUCTION

Vegetables are rich in minerals, vitamins, iron and dietary fibers that are linked to the maintenance of well-being of individuals [1]. In Europe, most of the public health institutions have run awareness campaigns about the importance of the consumption of vegetables and fruits in daily life [2]. Common daily vegetables includes carrots, lettuces, cucumbers, peppers, radishes, salad as well as other green vegetables that easily accessible at markets. Most of the microbes found on fruits and vegetables are soil inhabitants which are responsible for the maintaining of the ecological system in agricultural fields [3]. Exposure to the microbes can occur at all stages starting from pre harvesting, post harvesting, storage and at consumption step [3]. Study has showed that contaminated materials with non-pathogenic microbes show a various consequences on the quality of the produce since it's affecting the rate of the food spoilage [4]. The employment of the manures in agricultural sectors has a numerous beneficial to the plant`s growth and health. However, it promoted a number of pathogenic organisms to the plants such as *Listeria monocytogenes*, *Yersinia enterocolitica*, *Clostridium perfringens*, *Bacillus antracis*, *Salmonella spp*., *Klebsiella spp.* and *Escherichia coli* [5].

Previous studies have shown that the growing number of foodborne illness in recent years is associated with the increased of consumption of fresh produce since there are known as a host of pathogenic and non-pathogenic bacteria [6, 7]. According to Centers for Disease Control and Prevention (CDC), more than 50% of the outbreaks reported in the United State occurred in year the 1973 to 1997 were due to contaminated of fresh produce with *Salmonella spp*. [8]. Other studies also shown that the raw consumption and improperly cooked vegetables may contribute to the increased of outbreaks due to living human pathogens such as *L. monocytogenes, E. coli* and *Salmonella spp.* [9,10] . The common symptoms associated with *Salmonella* infections are fever, abdominal cramps, and diarrhea in individuals and high-risk of fatal to those with weak immune systems [9].

Culture based method is a conventional method for the identification of microorganisms or bacteria. Using this method, the bacteria was identified based

on their phenotypic characteristics, including Gram staining, morphology, culture requirements, and biochemical reaction [11]. However, these techniques have a lot of major limitations such as cannot be used for non-cultivable organisms, the biochemical characteristic of certain bacteria do not fit into patterns of any known genus and species and finally difficulty in identify the slow growing bacteria [11]. The limitation of culture based method was later overcome by molecular techniques with the introduction of the Polymerase Chain Reaction technology (PCR) in 1986 by Kary Mullis [12]. PCR is widely used in clinical biology due to its sensitivity, accuracy and more rapid compared to biochemical methods [12]. The applications of molecular techniques provide a reliable epidemiological data for tracing the source of human infection from foodborne illness cases [13]. Several techniques can be used to identify organism or bacteria such as restriction fragment length polymorphism (RFLP), amplified fragment length polymorphism (AFLP), pulse-field gel electrophoresis (PFGE) and DNA sequencing.

Recently, many studies were focusing on ribosomal RNA gene of mitochondrial DNA especially 16S rRNA gene. The size of 16S rRNA gene is about 1550 base pairs and the highly conserved sequence of 16S rRNA gene among bacteria and other organisms made this region become popular for identification of unknown organism using universal primer [14]. In addition, database for 16S rRNA gene for known bacteria are available established and consists of large deposited sequence from many sources that can be useful for identification and differentiating of unknown organism or bacteria [15]. The aim of this study was to identify the presence of organisms on vegetable samples through DNA sequencing of ribosomal gene.

MATERIALS AND METHODS

Sample collection

Sixteen (16) different types of vegetables were used in this study. All vegetable samples were purchased from the local wet market and supermarket in Kubang Kerian, Kelantan. The samples were then classified into two groups which were leafy (chinese broccoli, water spinach, chinese flowering cabbage, spinach, scallion, bok choy, coriander) and non leafy (eggplant, sweet potato, tomato, long bean, chili/ cayenne pepper, carrot, cauliflower, french beans, capsicum/ bell pepper).

Primer design

A new set of primers were designed based on 16S rRNA gene full sequence of selected bacteria. The 16S rRNA gene full sequences were available through the website of the National Center of Biotechnology Information (NCBI) (http://www.ncbi.nlm.nih.gov/). All the primers were manually designed and further confirmed using primer software (BioEdit ver. 4.0 software). The searched sequences were as follows: *Bacillus cereus (*NZ_CM000719.1), *Bacillus subtilis* (NC_000964.3), *Bacillus licheniformis* (NC_006270.3), *Escherichia coli* (NC_002695.1), *Erwinia amylovora* (NC_013961.1), *Erwinia carotovora* (NC_004547.2), *Listeria monocytogenes* (NC_003210.1), *Pseudomonas syringae* (NC_007005.1), *Pseudomonas fluorescens* (NC_016830.1), *Pseudomonas protegens* (NC_004129.6). In this study, two set of universal primer for 16S rRNA gene were used for amplification of unknown bacteria from vegetables samples. The details of the primers sequences are displayed in Table 1.

Sample Preparation and DNA extraction

All the vegetables were cut into small pieces and leave at ambient temperature for a few days until all the samples were completely dried. Prior to DNA extraction the dried samples were crushed into fine powder by using a mortar and pestle. As much 0.3 g of dried samples were used for DNA extraction using modified phenol-chloroform method as recommended by Healey *et al.* [16].

PCR optimisation

The PCR optimisation is necessary to obtain the efficient amplification of specific targets. The parameters need to be considered including cycles number, annealing temperature and the reagent concentrations as recommended by Stephenson and Abilock [17]. The gradient PCR technique was employed for both sets of primers at temperature 62ºC to determine the optimum annealing

Table 1: List of the universal primer for 16S rRNA gene sequence applied in PCR amplification of the unknown organism.

Primer	Primer Sequence (5' – 3')	Primer Set
BactF_355	ACT CCT ACG GGA GGC AGC	SET 1
BactR_722	ATC TAC GCA TTT CAC CGC TA	
BactF_951	GCA CAA GCG GTG GAG CAT GT	SET 2
BactR_1411	AAG GCC CGG GAA CGT ATT CA	

temperature for the primer set during the PCR process. The PCR reaction mix was prepared in 20 µL which consist of 2 µL of 10X PCR buffer $NH_4(SO4)_2$, 2 µL of the 25 mM $MgCl_2$, 0.32 µL of 10 mM dNTPs, 0.3 µL of Taq polymerase (5 U/µL) ,1 µL of 10 pmol of each primers (reverse and forward primers) ,11.38 µL of sterile deionized water (ddH_2O) and 2 µL of genomic DNA. The PCR was performed with initial denaturation at 95ºC for 3 minutes, followed by 30 cycles of denaturation at 95ºC for 3 minutes, primer annealing at 62ºC for 30 seconds, primer extension at 72ºC for 45 seconds and the final elongation at 72ºC for 5 minutes. The amplified products were then analyzed on 1% agarose gel with the loading volume of 3 µL of PCR product and 1 µL of Orange G dye and were allowed to run for 1 hour at 90V. The result obtained was visualized under UV light using gel documentation system (Vilbert Lourmat/Quantum). The annealing temperatures for each primer set were chosen based on the good DNA band intensity on the agarose gel.

PCR Amplification and DNA purification of 16S rRNA Gene

A total of 2 µL genomic DNA was used for PCR amplification using the previously described condition in this study. PCR product was detected by 1 % agarose gel electrophoresis, stained with 1.6 µL ethidium bromide and was allowed to run for 1 hour at 90V. The result obtained was visualized under UV light using gel documentation system (Vilbert Lourmat/Quantum). The PCR amplicon were purified using Gene ALL PCR SV kit (Helix Biotech, Malaysia.) by following manufacturer`s instructions.

Analysis of the DNA Sequence

The PCR products were sequenced using an automated DNA sequencer (Tech Dragon Ltd, Hong Kong, China). The raw DNA sequence data was analyzed using BioEdit ver.4.0 software. The treated DNA sequence then was BLAST using free software at National Center for Biotechnology Information (http://www.ncbi.nlm.nih.gov/) in order to identify the bacteria infected vegetable samples.

RESULTS

In this study, a total of 16 samples of dried vegetables were examined for identification of bacteria using newly designed primer of 16S rRNA gene. Based on PCR optimisation results, universal primer SET 2 show a good band intensity with less smear and nonspecific binding were generated at temperature 62ºC (Figure 1). PCR amplification of SET 2 (BactF_951 and BactR_1411,) produced amplicon at 460 bp (Figure 2). Meanwhile, amplification of SET 1 (BactF_355 and BactR_722) which produced amplicon at 367 bp (Figure 2), showed DNA band with more smear and non specific binding compare to PCR amplification of SET 2. Thus, this study has chosen universal primer of SET 2 (BactF_951 and BactR_1411) for PCR amplification of vegetable samples. Out of the 16 samples, 14 samples gave a positive result for the amplification of the 16S rRNA gene (Figure 3). Extracted DNA from sample french beans (S14) and coriander (S15) were failed to amplified using primer BactF_951 and BactR_1411 (SET 2).The failure of amplification also can be caused by the highly degraded genetic material into very small fragments. According to Golenberg *et al*. [18], the initial fragmentation of the template DNA grossly affected the PCR amplification product directly or indirectly by interfere the enzymatic reactions. All the 14 samples then were purified prior to DNA sequencing.

DNA sequencing result show out of the 14 samples, only 11 samples were accepted for further analysis. Three samples that fail for DNA sequencing are sweet potato (S6), tomato (S7) and chili (S9). Based on the electropherogram of the 3 samples, it is suggested that either the low DNA concentration of the purified PCR products or the presence of the impurities in the samples might be the main factors contributing to the failure of DNA sequencing. The unknown sequence profiles generated from the amplification of universal primer 16S rRNA gene further analysed using Basic Local Alignment Search Tool (BLAST) to identify the organism

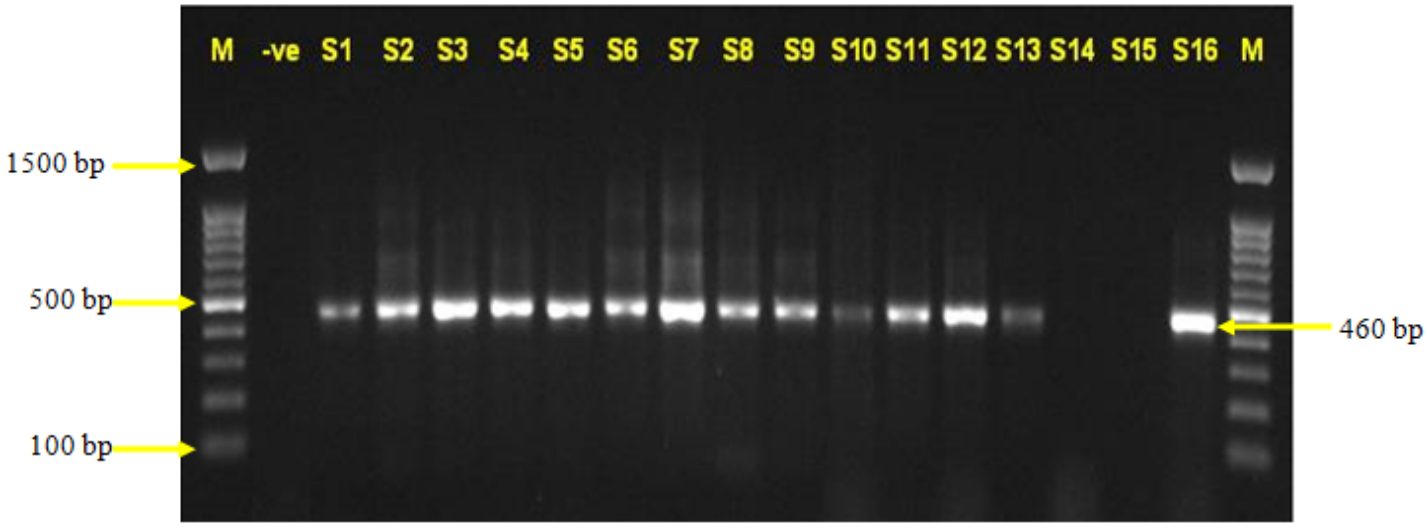

Figure 1: PCR optimisation of universal primer 16S rRNA of SET 2 at 460 bp (BactF_951 and BactR_1411).

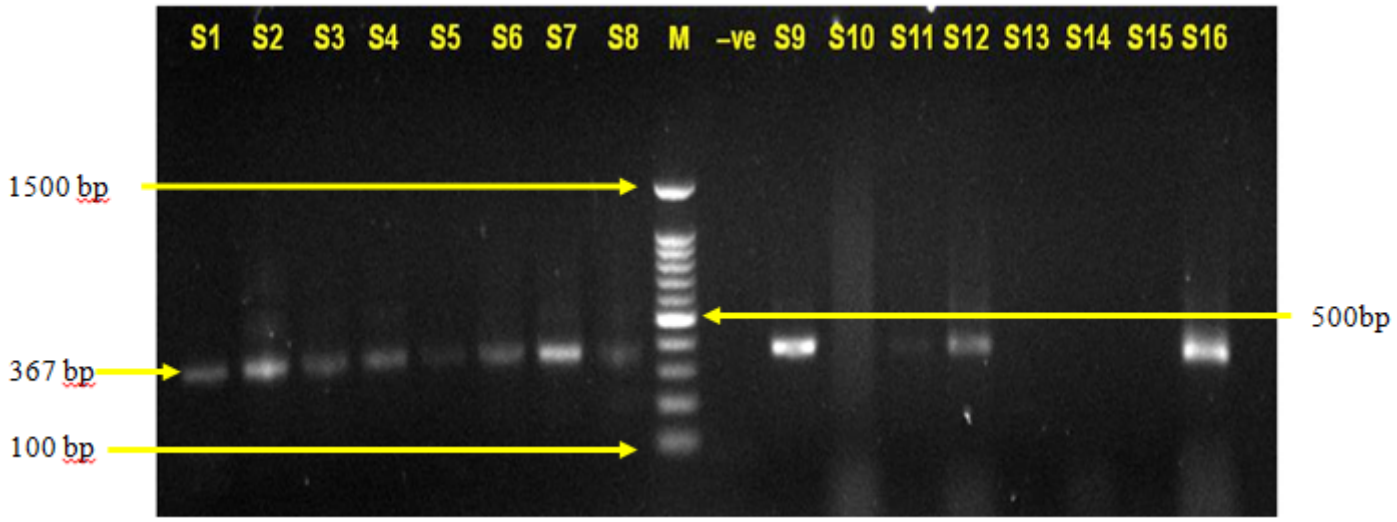

Figure 2: PCR optimisation of universal primer 16S rRNA gene of SET 1 at 367 bp (BactF_355 and BactR_722).

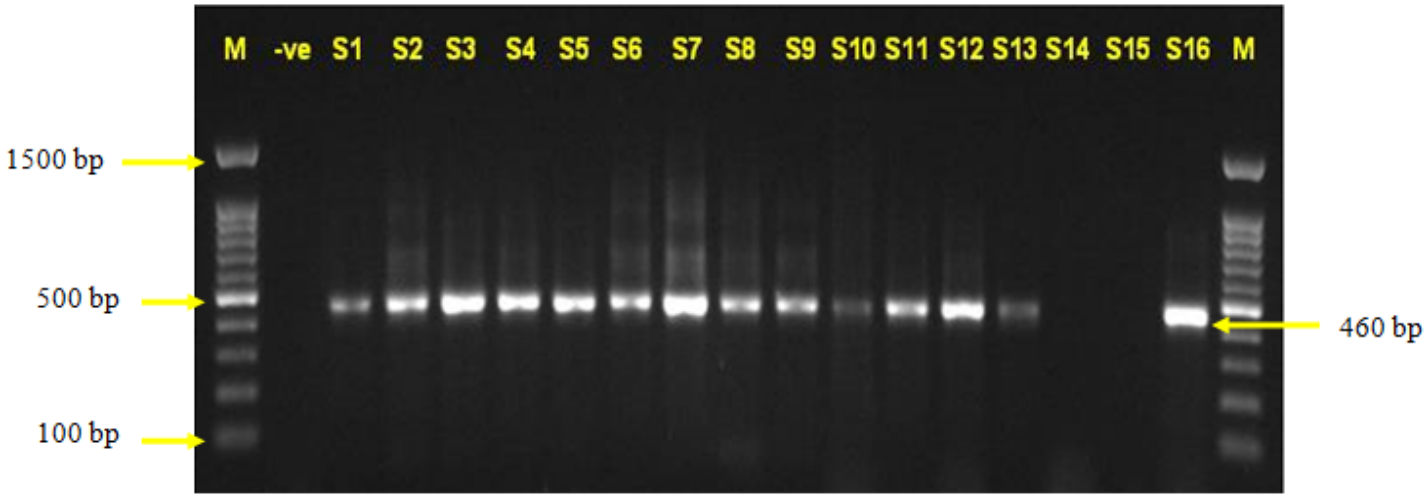

Lane M	: DNA ladder (100bp)	Lane S8	: Long beans
Lane -ve	: Negative control	Lane S9	: Chili
Lane S1	: Chinese broccoli	Lane S10	: Scallion
Lane S2	: Water spinach	Lane S11	: Capsicum
Lane S3	: Chinese flowering cabbage	Lane S12	: Cauliflower
Lane S4	: Spinach	Lane S13	: Pak choy/ Bok choy
Lane S5	: Eggplant	Lane S14	: French beans
Lane S6	: Sweet potato	Lane S15	: Coriander
Lane S7	: Tomato	Lane S16	: Carrot

Figure 3: Amplified PCR product of universal primer 16S rRNA gene SET 2 (BactF_951 and BactR_1411).

presence on the vegetable samples. Based on the Table 2, a diverse bacterial communities were identified from 11 samples, show that the successful of the newly designed universal primer 16S rRNA gene. The bacterial community such as *Bacterium, Cyanobacterium, Actinobacterium, Bacillales, Sphingomonadales, Carnobacterium, Trichodesmium sp.* and *Deinococcus sp.* were identified on the vegetable sample (Table 2). This finding is similar with other previous study reported by [19, 20,6, 21]. All the identified organisms are Gram positive of enteric bacterial. Although, most of the enteric bacteria are harmless and non pathogenic, however, precaution should be taken to avoid health problems. Interestingly, a long bean (S8) is the only vegetable sample was identified with one type of bacteria which is bacterium type. The main reason for that, it could be the long beans may have less contact with soil compared to other vegetable samples. All the vegetable samples were identified with bacterium type (Table 2). The word of bacterium is referring to the single unrecognized bacterium which is submitted by a research in the NCBI website. The unresolved bacteria type indicates that not enough information was generated using partial sequence of 16S rRNA gene to identify the bacteria.

All the identified bacteria from BLAST results were classified into phyla in order to observe the distribution of the bacteria community on the vegetable samples (Figure 4). As shown in Figure 4, five types of phyla were classified namely *Cyanobacteria, Deinococcus, Actinobacteria, Proteobacteria* and *Firmicutes.* The majority of the bacteria were belonging to the *Cyanobacteria* phylum ranging from 60% to 82% (Figure 4). The second common phyla are *Actinobacteria* and *Firmicutes* which ranging from 1-2 % respectively (Figure 4). Phylum *Deinococcus* only seen in a few vegetable samples such as water spinach (S2), spinach (S4), eggplant (S5) and capsicum (S11) with relative abundance ranged between 1-2 % (Figure 4). *Deinococcus sp.* is a bacterium that has a characteristic of highly resistant to environmental hazards [22]. Previous studies have shown that the *Deinococcus sp.* has been isolated from wet sources area such as river [23] and sewage [24]. Classification of phyla cannot be determined for long beans vegetable since there is no specific bacteria was identified (Figure 4).

Table 2: The list of bacteria identified on vegetable samples.

Vegetable names	**List of Bacteria**
Chinese broccoli (S1)	*Bacterium, Cyanobacterium, Actinobacterium, Bacillales Bacterium, Sphingomonadales Bacterium (proteobacteria), Carnobacterium, Trichodesmium sp.*
Water spinach (S2)	*Bacterium, Cyanobacterium, Actinobacterium, Sphingomonadales Bacterium (proteobacteria), Carnobacterium, Trichodesmium sp., Deinococcus sp.*
Chinese flowering cabbage (S3)	*Bacterium, Cyanobacterium, Actinobacterium, Bacillales Bacterium, Sphingomonadales Bacterium (proteobacteria), Carnobacterium, Trichodesmium sp.*
Spinach (S4)	*Bacterium, Cyanobacterium, Actinobacterium, Sphingomonadales Bacterium (proteobacteria), Carnobacterium, Trichodesmium sp., Deinococcus sp.*
Eggplant (S5)	*Bacterium, Cyanobacterium, Actinobacterium, Sphingomonadales Bacterium (proteobacteria), Carnobacterium, Trichodesmium sp., Deinococcus sp., Bacillales Bacterium.*
Long beans (S8)	*Bacterium*
Scallion (S10)	*Bacterium, Cyanobacterium, Actinobacterium, Sphingomonadales Bacterium (proteobacteria), Carnobacterium, Trichodesmium sp.*
Capsicum (S11)	*Bacterium, Cyanobacterium, Actinobacterium, Sphingomonadales Bacterium (proteobacteria), Carnobacterium, Trichodesmium sp., Deinococcus sp.*
Cauliflower (S12)	*Bacterium, Cyanobacterium, Actinobacterium, Sphingomonadales Bacterium (proteobacteria), Carnobacterium, Trichodesmium sp.*
Pak choy/ Bok choy (S13)	*Bacterium, Cyanobacterium, Actinobacterium, Sphingomonadales Bacterium (proteobacteria), Carnobacterium, Trichodesmium sp.*
Carrot (S16)	*Bacterium, Cyanobacterium, Actinobacterium, Sphingomonadales Bacterium (proteobacteria), Carnobacterium, Trichodesmium sp.*

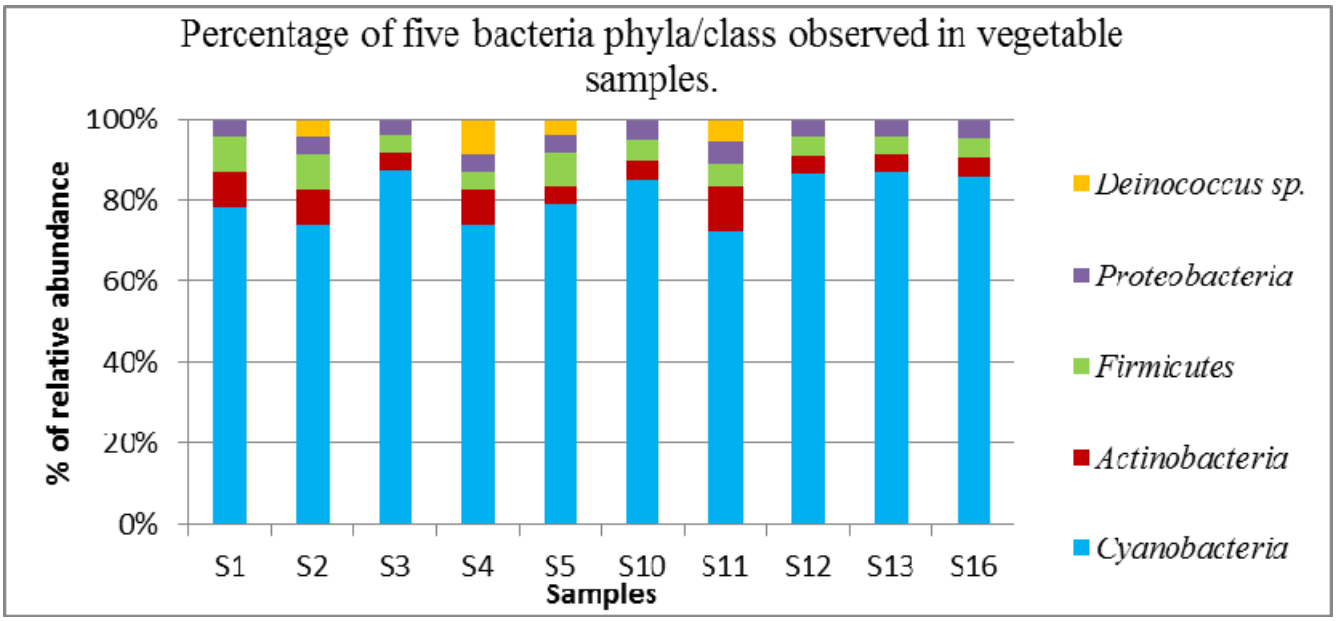

Figure 4: The graph shown the percentage of bacteria phyla/class observed in vegetable samples.

DISCUSSIONS

The abundance of microbial diversity was analyzed deeper into taxonomic level. Phyla *Deinococcus, Firmicutes* and *Cyanobacteria* were attributed into a genus level; meanwhile phyla *Actinobacteria* and *Proteobacteria* were assigned into a family level. *Carnobacterium* and *Bacillales bacterium* are classified under *Firmicutes* phylum. Meanwhile, *Deinococcus sp.* is the genus for *Deinococcus* phylum and *Trichodesmium sp*. is the genus belong to *Cyanobacteria* phylum [25,26]. *Trichodesmium sp.* was usually found in tropical and subtropical oceans. However, as reported by Prufert-Bebout *et al*. [27], *Trichodesmium sp.* was growing successfully in culture laboratory for over 1 year by modifying the medium with seawater and proper handling technique. This suggests that the bacteria can be introduced into different environment as long as the requirement nutrients were fulfilled constantly. *Actinobacterium* family was classified into the most dominant bacteria under the *Actinobacteria* phylum. Similarly, *Sphingomonadales* family was belong to the class *Proteobacteria* classified under *Proteobacteria* phylum [28]. The *Cyanobacteria* phylum was the most prominent found since these bacteria were introduced into vegetables by nitrogen fixing bacteria that originated from soils and water [27]. The vegetables can be exposed to the *Cyanobacterium sp.* during pre-harvest and post-harvest process. It has been reported that the *Cyanobacterium* contaminated the irrigation water during pre-harvest process by producing bioactive compounds like cyanotoxins which causing serious illness if directly consumed [29].

The finding also shows chinese broccoli (S1), chinese flowering cabbage (S3), scallion (S10), capsicum (S12), pak choy/ bok choy (S13) and carrot (S16) were identified with bacteria that classified under the phyla *Proteobacteria, Firmicutes and Actinobacteria* which are responsible for spoilage and deterioration of fresh vegetables [6,21] (Table 2 and Figure 4). Study conducted by Rinland and Gomez [30], described bacteria under these phyla (*Proteobacteria, Firmicutes* and *Actinobacteria*) involved in degradation of different biomass wastes on onion. This study also revealed that the bacteria under *Proteobacteria* and *Firmicutes* phyla were less dominant found on vegetable samples (Table 2 and Figure 4). This finding was contrast to Lopez-Velasco *et al*. [20], since those bacteria phyla are frequently observed in spinach. Pathogenic bacteria or human pathogen such as *Salmonella sp.*, *Listeria sp.* and *E. coli O157:H7* were not detected in this study. This might be due to the presence of the *Actinobacterium* and *Carnobacterium* that suppress the plant pathogens since both of these bacteria have insecticidal and antimicrobial characteristics [31, 32]. The trends and types of bacteria identified from this study were found to be consistent and does not represent all the bacterial communities that associates with plants. Jackson *et al.* [21] pointed out that the different types of fresh produce would have distinct bacterial communities which can be found on any parts of plants like leaves, seeds, or roots. However, certain fresh vegetables could exhibit more similar bacterial communities such as spinach, sprouts and lettuce [21].

CONCLUSION

This study has shown the application of universal primer 16S rRNA gene in identifying the bacterial community from vegetable samples. A newly designed universal primer based on 16S rRNA gene of selected bacteria was successfully amplified 460 bp partial sequence of 16S rRNA gene. The presence of bacteria diversity on vegetable samples indicate that every stage involved starting from pre-harvest process till the end process to the consumer has probability to introduce bacteria into vegetable samples. Though all the identified bacteria were non pathogen and harmless to human being but in certain situation these types of bacteria also can cause illnesses to human such as stomach uncomfortable, vomiting, dizziness and diarrhea. Therefore, the precaution should be taken during preparing vegetable such as wash under the clean water, avoid taking raw vegetables in the menu and properly cooked vegetable. The results also proved that the identification of bacteria using the partial 16S rRNA gene was possibly identified directly from samples without performing culture method. In summary, the molecular approaches that applied in identification of bacterial community from vegetable samples are offering more sensitive, rapid and robust method compared to standard laboratory culture.

ACKNOWLEDGEMENT

The authors would like to express special thanks to Faculty of Health Sciences, Universiti Sains Malaysia (Health Campus) for funding this research (Grant No 304/PPSK/61313109).

REFERENCES

1. Prasanna, V., Prabha, T. N., & Tharanathan, R. N. (2007). Fruit Ripening Phenomena–An Overview. *Critical Reviews in Food Science and Nutrition , 47* (1), 1-19.
2. Abadias, M., Usall, J., Anguera, M., Solsona, C., & Viñas, I. (2008). Microbiological Quality of Fresh, Minimally-Processed Fruit and Vegetables and Sprouts From Retail Establishments. *International Journal of Food Microbiology , 123*, 121–129.
3. Barth, M., Hankinson, T. R., Zhuang, H., & Breidt, F. (2009). Compendium of the Microbiological Spoilage of Foods and Beverages. In W. H. Sperber, & M. P. Doyle, *Compendium of the Microbiological Spoilage of Foods and Beverages* (pp. 135 -183). United States: Food Microbiology and Food Safety.
4. Leff, J. W., & Fierer, N. (2013). Bacterial Communities Associated with the Surfaces of Fresh Fruits and Vegetables. *PLoS ONE , 3* (8), e59310.
5. Eni, A., Oluwawemitan, I., & Solomon, O. (2010). Microbial Quality of Fruits and Vegetables Sold in Sango Ota, Nigeria. *African Journal of Food Science , 4* (5), 291-296.
6. Rastogi, G., Sbodio, A., Tech, J. J., Suslow, T. V., Coaker, G. L., & Leveau, J. H. (2012). Leaf Microbiota in An Agroecosystem: Spatiotemporal Variation in Bacterial Community Composition on Field-Grown Lettuce. *International Society for Microbial Ecology , 6*, 1812–1822.
7. Zahra, S., Nejib, G., Abdullah, M., Ismail, M., & Baby, S. (2016). Hiding in Fresh Fruits and Vegetables: Opportunistic Pathogens May Cross Geographical Barriers. *International Journal of Microbiology* , 1-14.
8. Buck, J. W., Walcott, R. R., & Beuchat, L. R. (2003). Recent Trends in Microbiological Safety of Fruits and Vegetables. *Plant Management Network , 110*, 200-210.
9. Fatica, M. K., & Schneider, K. R. (2011). Salmonella and Produce: Survival in the Plant Environment and Implications in Food Safety. *Virulence , 2* (6), 573-579.
10. Critzer, F. J., & Doyle, M. P. (2010). Microbial Ecology of Foodborne Pathogens Associated with Produce. *Current Opinion in Biotechnology , 21* (2), 125-130.
11. Woo, P. C., Ng, K. H., Lau, S. K., Yip, K. T., Fung, A. M., Leung, K. W., et al. (2003). Usefulness of the MicroSeq 500 16S Ribosomal DNA-Based Bacterial Identification System for Identification of Clinically Significant Bacterial Isolates with Ambiguous Biochemical Profiles. *Journal of Clinical Microbiology , 41* (5), 1996–2001.
12. Mullis, K. B. (1990). The Unusual Origin of the Polymerase Chain Reaction. *Scientific American , 262* (4), 56-61.
13. Adzitey, F., Huda, N., & Rahmat Ali, G. R. (2013). Molecular Techniques for Detecting and Typing of Bacteria, Advantages and Application to Foodborne Pathogens Isolated From Ducks. *Biotechnology , 3* (2), 97–107.
14. Yang, L., Tan, Z., Wang, D., Xue, L., Guan, M. X., Huang, T., et al. (2014). Species Identification through Mitochondrial rRNA Genetic Analysis. *Scientific Reports , 4* (4089), 1-12.
15. Breeze, R. G., Budowle, B., & Schutzer, S. E. (2005). *Microbial Forensics.* Waltham, MA: Academic Press.
16. Healey, A., Furtado, A., Cooper, T., & Henry, R. J. (2014). Protocol : A Simple Method for Extracting Next-Generation Sequencing Quality Genomic DNA From Recalcitrant Plant Species. *Plant Methods , 10* (21), 1-8.
17. Stephenson, F., & Abilock, M. (2012). *Optimizing the Polymerase Chain Reaction Student Guide.* Hayward, CA: Life Technologies and Applied Biosystems/ BABEC Educational PCR Kits.

18. Golenberg, E. M., Bickel, A., & Weihs, P. (1996). Effect of Highly Fragmented DNA on PCR. *Nucleic Acids Research , 24*, 5026-5033.
19. Carder, P. A. (2010). *Microbial Communities of Spinach at Various Stages of Plant Growth From Seed to Maturity.* Virginia Tech: Thesis, Master in Science dissertation.
20. Lopez-Velasco, G., Welbaum, G. E., Boyer, R. R., Mane, S. P., & Ponder, M. A. (2011). Changes in Spinach Phylloepiphytic Bacteria Communities Following Minimal Processing and Refrigerated Storage Described Using Pyrosequencing of 16S rRNA Amplicons. *Journal of Applied Microbiology , 110*, 1203–1214.
21. Jackson, C. R., Randolph, K. C., Osborn, S. L., & Tyler, H. L. (2013). Culture Dependent and Independent Analysis of Bacterial Communities Associated with Commercial Salad Leaf Vegetables. *BMC Microbiology , 13*, 274 - 286.
22. Krisko, A., & Radman, M. (2013). Biology of Extreme Radiation Resistance: The Way of Deinococcus radiodurans. *Cold Spring Harbor Perspectives in Biology , 5* (7), a012765.
23. Lee, J. J., Lee, Y. H.,Park, S. J., Lim, S., Jeong, S.W., Lee, S. Y., Park, S., Choi, H. W., Kim, M. K., Jung, H. Y. (2016). *Deinococcus sedimenti sp. nov.* Isolated from river sediment. *Journal of Microbiology*, 54 (12) , 802-808.
24. Srinivasan, S., Lim, S., Joe, M., Kim, M. K., & Lee, M. (2012). Deinococcus daejeonensis sp. nov., Isolated from Sludge in a Sewage Disposal Plant. *International Journal of Systematic and Evolutionary Microbiology , 62* (6), 1265-1270.
25. Makarova, K. S., Aravind, L., Wolf, Y. I., Tatusov, R. L., Minton, K. W., Koonin, E. V., et al. (2001). Genome of the Extremely Radiation-Resistant Bacterium Deinococcus radiodurans Viewed from the Perspective of Comparative Genomics. *Microbiology and Molecular Biology Reviews , 65* (1), 44-79.
26. Bergman, B., Sandh, G., Lin, S., Larsson, J., & Carpenter, E. J. (2013). Trichodesmium – A Widespread Marine Cyanobacterium With Unusual Nitrogen Fixation Properties. *FEMS Microbiology Reviews , 37*, 286–302.
27. Prufert-Bebout, L., Paerl, H. W., & Lassen, C. (1993). Growth, Nitrogen Fixation, and Spectral Attenuation in Cultivated Trichodesmium Species. *Applied and Environmental Microbiology , 59* (5), 1367-1375.
28. Reddy, G. S., & Garcia-Pichel, F. (2007). Sphingomonas mucosissima sp. nov. and Sphingomonas desiccabilis sp. nov., From Biological Soil Crusts in the Colorado Plateau, USA. *International Journal of Systematic and Evolutionary Microbiology, 57*, 1028–1034.
29. Cordeiro-Araujo, M. K., Chia, M. A., Hereman, T. C., Sasaki, S. S., & Bittencourt-Oliveira, M. C. (2015). Selective Membrane Permeability and Peroxidase Activity Response of Lettuce and Arugula Irrigated with Cyanobacterial-Contaminated Water. *Environmental Earth Science , 74*, 1547–1553.
30. Rinland, M. A., & Gomez, M. A. (2015). Isolation and Characterization of Onion Degrading Bacteria From Onion Waste Produced in South Buenos Aires Province, Argentina. *World Journal of Microbiology and Biotechnology , 31*, 487–497.
31. Hoenigl, M., Grisold, A. J., Valentin, T., Leitner, E., Zarfel, G., Renner, H., et al. (2010). Isolation of Carnobacterium sp. from A Human Blood Culture. *Journal of Medical Microbiology , 59*, 493–495.
32. Shivlata, L., & Satyanarayana, T. (2015). Thermophilic and Alkaliphilic Actinobacteria: Biology and Potential Applications. *Frontiers in Microbiology , 6* (1014), 1-13.

The International Journal of Medicine and Sciences ***4*** *(1) 2019 : 27-32*

Case Report

IDIOPATHIC FROSTED BRANCH ANGIITIS IN PAEDIATRIC PATIENTS: CASE SERIES

Tanusha Dorairaja*[1,2], Goh Siew Yuen [1], Jamalia Rahmat [1]

[1]Department of Ophthalmology, Hospital Kuala Lumpur, Jalan Pahang, 50586 Kuala Lumpur, Malaysia.
[2]Department of Ophthalmology, Faculty of Medicine, University Malaya Medical Centre, Jalan Universiti, 59100 Kuala Lumpur, Malaysia.

ARTICLE INFO

Corresponding author:
Dr. Tanusha Dorairaja

Email address:
d_tanusha@hotmail.com

Received:
March 2019
Accepted for publication:
May 2019

Keywords:

Frosted branch angiitis
retinal vasculitis
macular oedema
systemic corticosteroids
intravenous acyclovir

ABSTRACT

Frosted branch angiitis is typically a bilateral diffuse retinal periphlebitis that can occur in a number of varying condition. It is a rare entity and a diagnosis of exclusion. We report a case series of primary idiopathic frosted branch angiitis in 2 young healthy girls with different ocular manifestations. Both girls presented with symptoms of sudden severe blurring of vision with only perception to light. In Case 1, patient had left reactive cervical lymphadenopathy and in Case 2, patient presented with both eye redness and mild pain. There were no systemic association in both cases. Fundus examination revealed retinal vasculitis with perivascular exudates and disc hyperemia in both patients, however Case 2 showed dense vitritis and retinal hemorrhages as well. Blood investigations, cultures, infection screening and TORCHES were unremarkable in both cases. Ocular coherence tomograpghy (OCT) in both patients showed retinal edema with subretinal fluid in the earlier part of disease, however in Case 2, the disease resolved with foveal atrophy. Both patients were treated with Intravenous Methylprednisolone and Intravenous Acyclovir followed by tapering dose of oral corticosteroids and acyclovir for 6 week duration. Following treatment, the uveitis completely resolved in Case 1, however Case 2 was complicated with posterior subcapsular cataract and foveal atrophy. On subsequent follow up, Case 1 had good visual outcome and Case 2 had poorer vision due to cataract and foveal atrophy. Frosted branch angiitis shows an excellent response to systemic corticosteroid and has a good prognosis with early treatment.

INTRODUCTION

Frosted branch angiitis (FBA) was first described in Japanese literature by Ito in 1976 in a 6-year-old child [1]. It is a rare entity with approximately 100 cases described in literature till 2017. The great majority (75%) of patients are Japanese, indeed it was not until 1988 that any patient outside Japan was reported [2]. The diagnosis is made clinically with typical periphlebitis, veins being involved more commonly than arteries in a pattern of frosted branches of a tree supplemented by fundus fluorescein angiography findings [1]. We report the ocular manifestation, management and visual outcome of 2 patients with frosted branch angiitis seen in our centre.

CASE SERIES

Case 1

An 8-year-old girl with no known medical illness was referred from Hospital Melaka to our clinic with a history of sudden onset of bilateral blurring of vision. There was history of painless neck swelling on the left side associated with fever 2 days prior to the blurring of vision. There was no history of upper respiratory tract infection or diarrhea. On examination, vision was vague perception to light in both eyes. Both pupil were dilated with poor reaction to light. The anterior chamber showed 1+ cells with iris pigments on lens. Funduscopy revealed clear media with hyperemic optic discs. There were dilated and tortuous retinal vessels with perivascular sheathing and dull foveal reflex (Figure 1, 2).

Optical Coherent Tomography of both maculae showed the presence of subretinal fluid. The diagnosis of bilateral frosted branch angiitis was made. Hematological investigations revealed normal hemoglobin of 11.3 g/dL and a normal white cell count of 7.6×10^3/mL. Erythrocyte sedimentation rate (ESR) was slightly elevated, 51 mm/h. Serology for Toxoplasma, Hepatitis B, C and

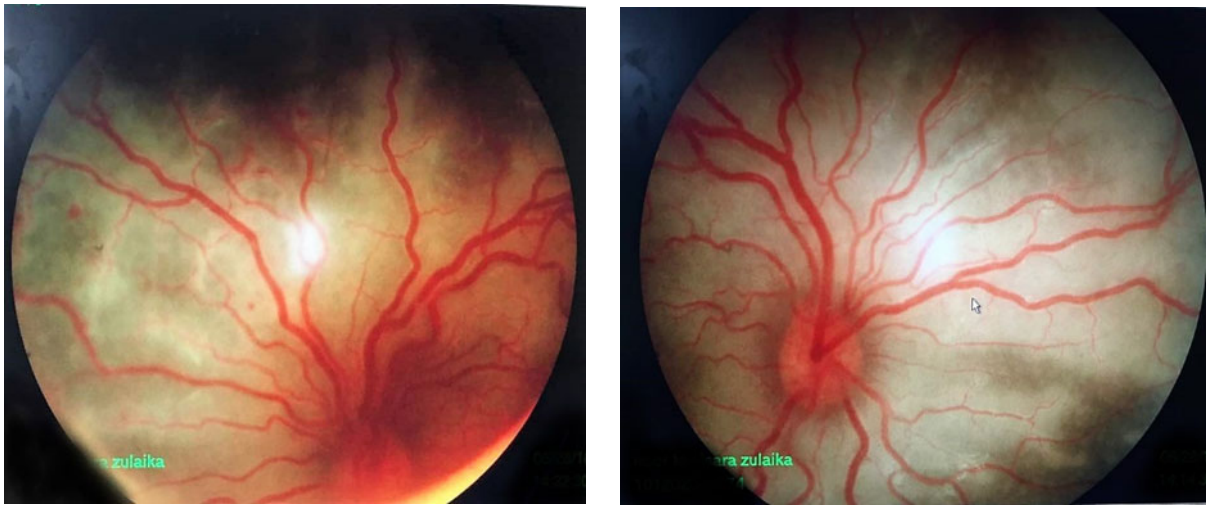

Figure 1. Fundi of both eyes at initial presentation showing hyperemic discs, dilated and tortuous vessels with perivascular sheathing, extensive retinal oedema involving the macula.

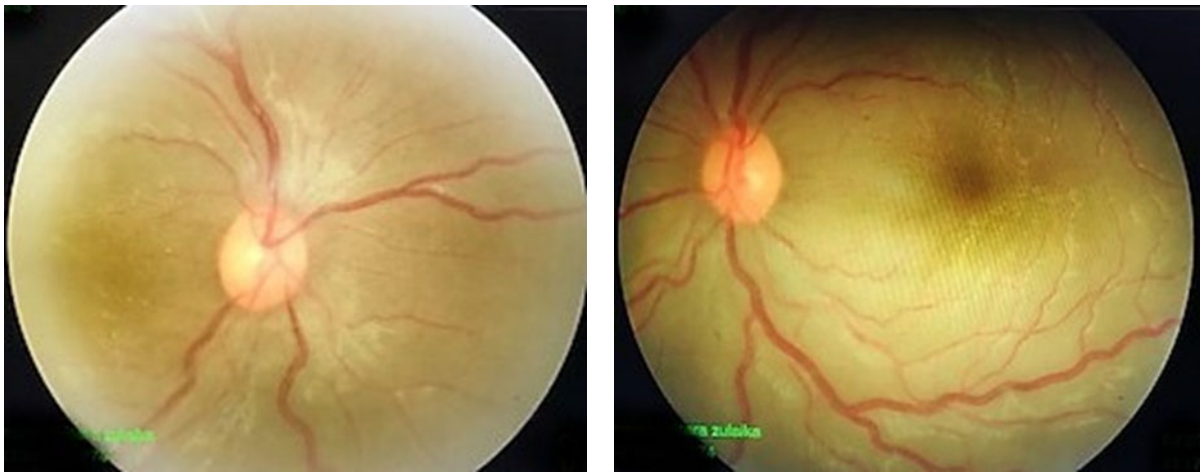

Figure 2: Appearance of both fundi at one week following treatment showing improvement.

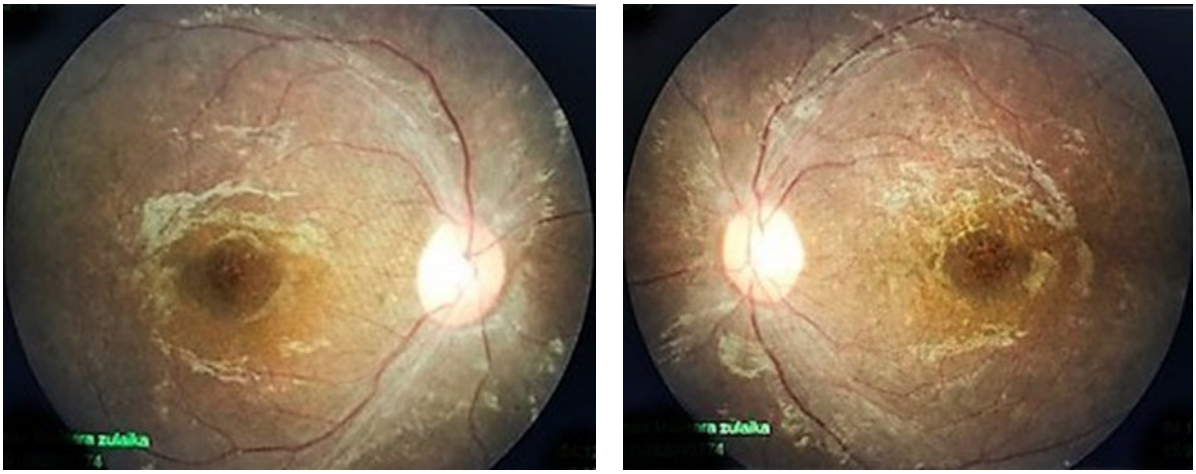

Figure 3: At 6 months post treatment : the vessels were attenuated and there were pigmentary changes at the periphery.

Human immunodeficiency Virus (HIV) were all non reactive, however Mantoux test was 0 mm. Ultrasound of neck revealed left cervical lymphadenopathy, Chest X ray and Contrast enhanced computed tomography (CECT) of orbits were normal. Histopathology examination of biopsy of left neck lymph node revealed reactive lymphadenitis. The patient was started on Gutt Prednisolone acetate 1% hourly and Intravenous (IV) Acyclovir infusion 20 mg/ kg three times a day for 1 week followed by oral Acyclovir at the same dose four times a day for the next 6 weeks. A 3-day course of IV Methylprednisolone was administered at 10mg/kg followed by oral prednisolone at a dose of 1 mg/ kg and slowly tapered over the next 2 months. There were resolution of severe vasculitis over the next 6 weeks. (Figure 3). The best corrected vision (BCVA) was 6/18 and 6/15 in the right and left eye respectively at 6 months.

Case 2

A 7-year-old girl with no known medical illness was referred from Hospital Seremban to our eye clinic with sudden onset of blurring of vision in both eyes of 4 days duration, associated with redness and mild pain. There were no history of fever, upper respiratory tract infection or diarrhea. On ocular examination, vision were perception to light bilaterally. There were intense inflammation in both eyes evidenced by ciliary injection and anterior chamber reaction. There were 4+ cells, 360 degrees of broken posterior synechiae and the presence of posterior subcapsular cataract. Otherwise, there were no keratic precipitates or iris nodules seen. Funduscopy revealed hazy media due vitritis, hyperemic optic discs with macula edema. There were tortuous and sclerosed vessels with arteritis, perivascular sheathing and retinal hemorrhages in all quadrants(Figure 4, 5, 6,7). Macular OCT showed foveal atrophy with loss of inner segment (Figure 8). The

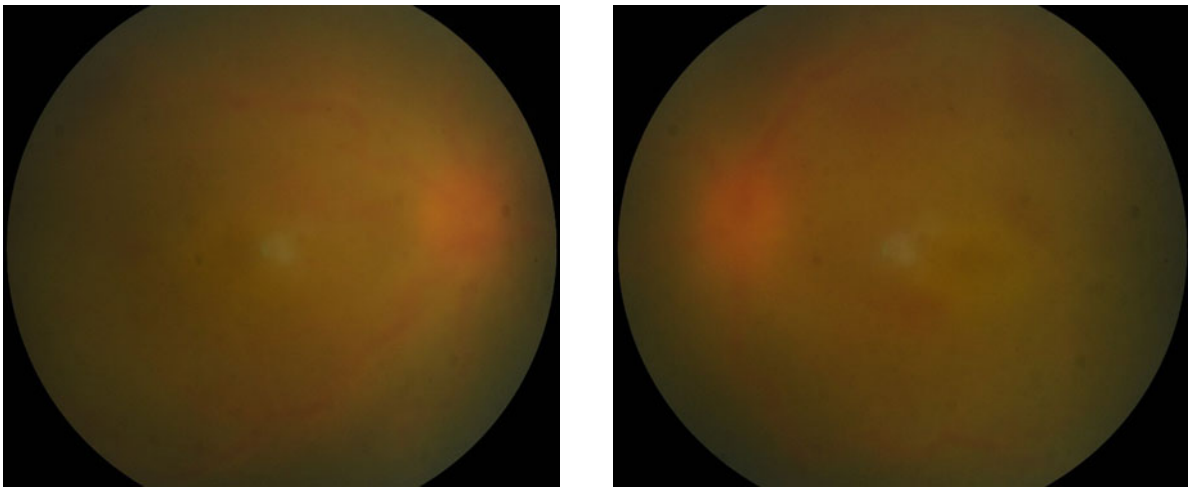

Figure 4 : Fundus photograph showing hazy view of both fundi at presentation.

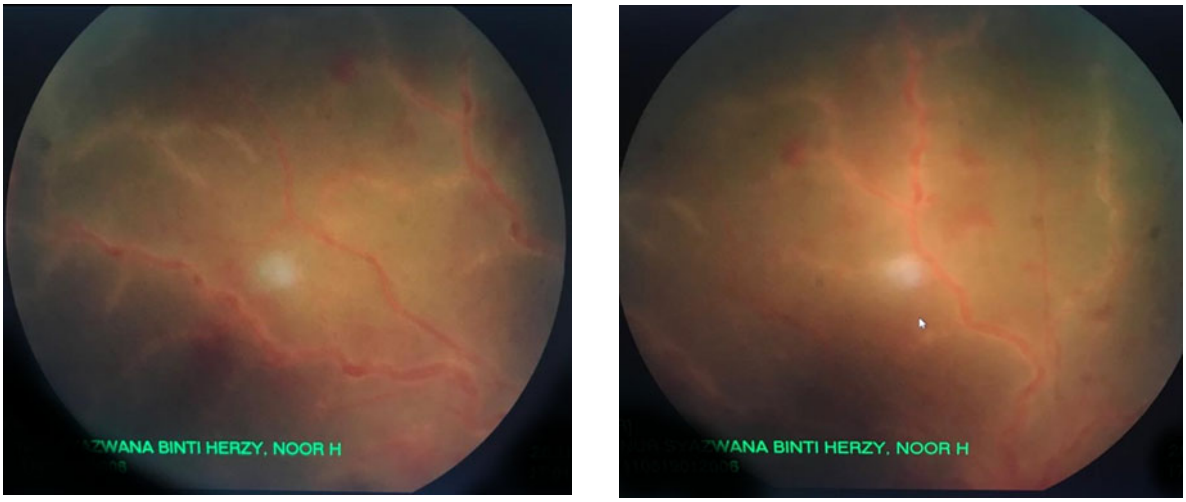

Figure 5. Fundus photograph of superior quadrants of both eyes showing hazy media due to vitritis, hyperemic disc, tortuous and sclerosed vessels with perivascular sheathing and retinal hemorrhages.

diagnosis of bilateral frosted branch angiitis was made. Hematology investigations revealed normal hemoglobin 14.1 gm/dL and a normal white cell of $8.4x10^3$/mL, full blood picture was normal, erythrocyte sedimentation rate (ESR) was 45 mm/h. The serology for TORCHES, Hepatitis B, C and HIV was non reactive. Mantoux test was 0 mm . Blood and urine cultures were negative. We administered intravenous Acyclovir infusion 500mg/m^2 three times a day for 1 week followed by oral acyclovir at the same dose four times a day for the next 6 weeks. IV Methylprednisolone was given at 10mg/kg three times per day for 3 days followed by oral prednisolone at a dose of 1 mg/ kg which was slowly tapered over 2 months. Patient also received topical Prednisolone acetate 1% hourly and prophylactic topical Ciprofloxacin 2- hourly, and topical Tropicamide. There were resolution of the severe vasculitis (Figure 7) over the next 6 weeks however patient developed posterior subcapsular cataract and foveal atrophy . Best corrected visual acuity were 6/60 in both eyes.

DISCUSSION

Frosted Branch Angiitis (FBA) predominantly affects the young and fit individuals. There appears to be a bimodal age distribution, with one peak in childhood and a second in the third decade of life. There has been a preponderance of females (61%) to males (39%) [2]. In our case series, both our cases were seen in healthy young female patients.

The most common presenting symptoms of FBA are subacute visual loss, floaters and flashes of light. The visual acuity may be reduced to perception of light. Associated systemic symptoms

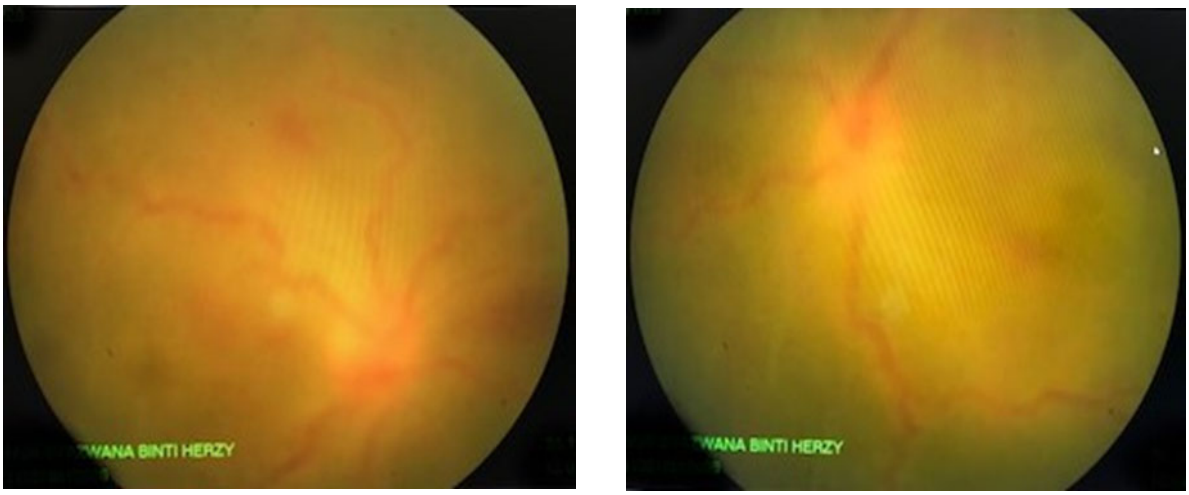

Figure 6: Fundus photograph on Day 3 of treatment.

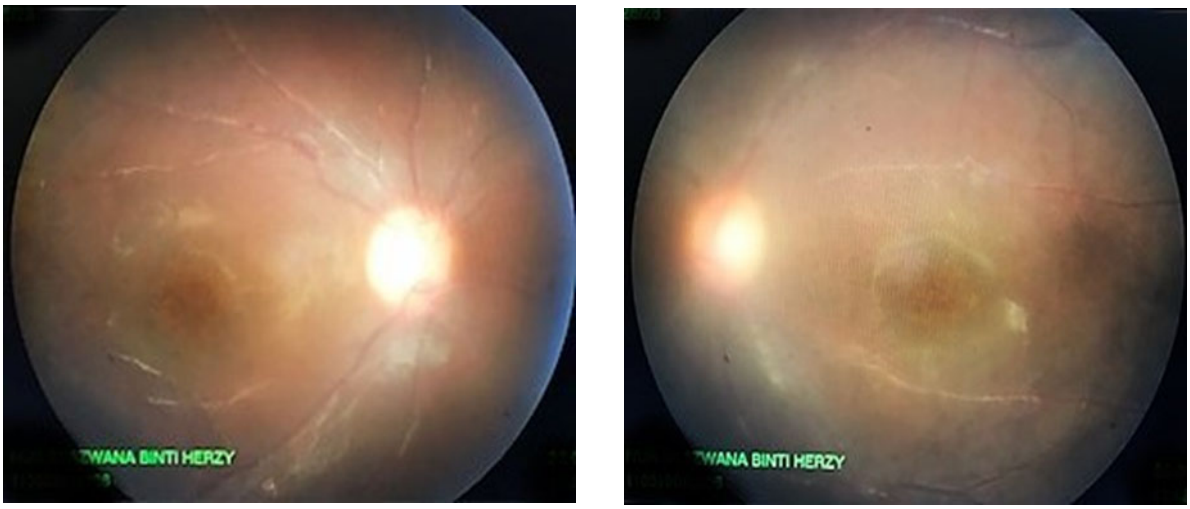

Figure 7: Fundus photograph after 6 weeks of treatment showing minimal vitritis, attenuated vessels with resolution of perivascular sheathing and macula scar.

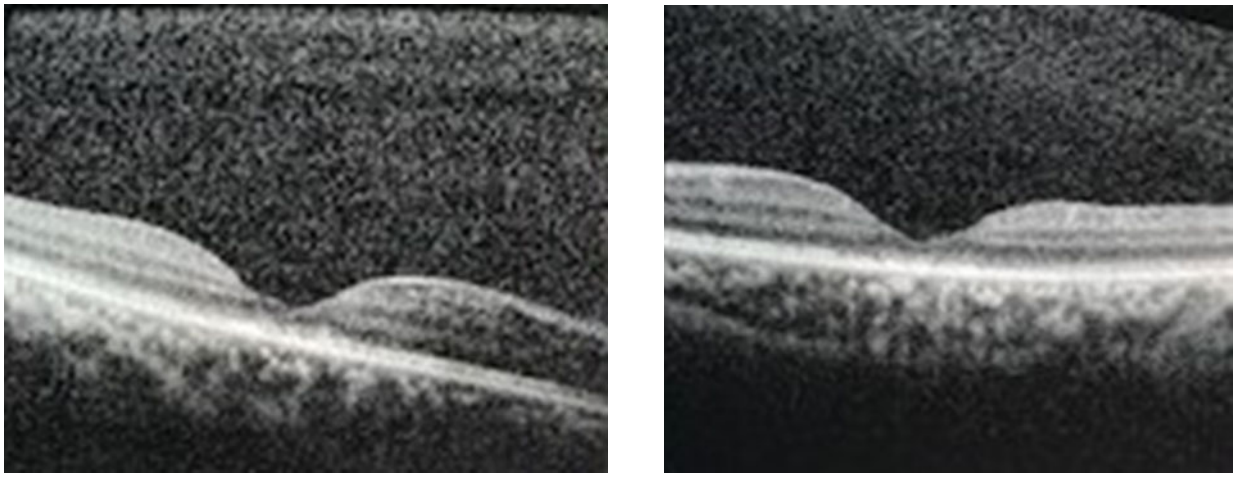

Figure 8: OCT of the right and left macula showing foveal atrophy with loss of inner segment.

are non-specific, such as flu-like syndrome including upper respiratory infection, sore throat, fever and malaise, back pain and headache. Most patients (75%) have bilateral disease [2,3] . Both our patients presented with sudden onset of blurring of vision in both eyes with perception to light.

Frosted branch angiitis can be an idiopathic disorder or can be associated with ocular and systemic diseases. Cytomegalovirus (CMV) retinitis, Acquired immune deficiency syndrome (AIDS) retinitis and Toxoplasma chorioretinitis are the most frequent ocular associations, while systemic lupus erythematosus, Crohn's disease, large cell lymphoma and acute lymphoblastic leukemia have been described as systemic disorders associated with frosted branch angiitis [3]. In both our cases, there were no systemic causes identified, though the ESR in both cases were moderately elevated, while zero reading for Mantoux were most likely due to the corticosteroid administered.

The cause of FBA is unknown. The typical onset of FBA after a prodromal illness has led to the suggestion of a hypersensitivity reaction to various infective agents, which may initiate FBA via a common pathway, possibly of immune-complex deposition [3].

Based on the underlying pathology, Kleiner suggested classifying patients into three different subgroups. The first group comprises patients affected by lymphoma and leukemia that can present with a frosted branch-like appearance in the fundus. The second group includes patients with associated autoimmune or infectious diseases which presented with FBA as a clinical sign of the underlying disease. Cytomegalovirus has been found to be the most common underlying infectious pathology followed by toxoplasmosis. These cases may show focal retinitis in addition to the vasculitis. Among autoimmune diseases, Behcet's disease is most frequently associated with FBA. The third group comprises patients with no identifiable cause and is classified as having primary idiopathic FBA. Patients with primary idiopathic FBA tend to be of younger age group, with bilateral involvement [2,3] .

Typically FBA has a striking fundus appearance of bilateral diffuse retinal vasculitis with a 'frosted' quality due to the perivascular exudate. Mild to moderate iritis with vitritis is common, as is retinal oedema. Intraretinal haemorrhages and punctate hard exudates are only occasionally seen. Papillitis, if present, is usually mild. Both our cases showed diffuse retinal vasculitis with perivascular exudates and disc hyperemia. However in case 2,the patient also had intense vitritis and retinal hemorrhage. In Case 1, OCT showed macula and retinal edema with subretinal fluid, however in Case 2, patient had foveal atrophy. Fluorescein angiography in case 2 was near normal in the early phase, but there was late leakage from the larger affected retinal vessels. In the recovery phase, microaneurysms have been described. The vasculitis is usually nonocclusive. Visual field analysis reveals constriction or relative central field defects that improve after clinical resolution. The latter are thought to be due to macular oedema [1,4,5,6].

Electrophysiology has shown a reduction in the amplitudes of the electroretinogram (ERG), electrooculogram (EOG) and visually evoked response (VER). This would be consistent with a widespread dysfunction of the retina, pigment epithelium and optic nerve. The EOG and VER may return to normal, but the ERG changes have generally persisted beyond convalescence, suggesting permanent retinal damage [1,6].

Complications include retinal vein or artery occlusion, macular epiretinal membrane formation, macula scarring, diffuse retinal fibrosis, retinal tear

formation, vitreous haemorrhage, optic disc atrophy and peripheral atrophic retinal lesions [1,5]. In our patients, Case 1 showed peripheral atrophic retinal changes and in Case 2 there was macula atrophy. Nevertheless, despite the severe retinal appearance, the prognosis is usually good, with rapid recovering of visual acuity after prompt systemic corticosteroid treatment. Visual field and electrophysiological tests return completely normal after one or two months from the disease onset [3,6].

There is no definite treatment protocol for this disease. In most of the previous studies no medication apart from corticosteroids were given, whereas some had opted a combination of corticosteroids and acyclovir. We observed good response with combination of acyclovir and corticosteroids in our cases. Following 6 weeks of therapy, the anterior uveitis, vitritis, and vasculitis completely regressed, leaving minimal morphological sequelae. The disease is frequently limited to an isolated acute episode, although rare cases of recurrence have been described [3].

CONCLUSION

Frosted branch angiitis is typically a bilateral diffuse retinal periphlebitis that may occur in a number of varying conditions. It is a diagnosis of exclusion with characteristic clinical presentation and typically affects children and younger adults. Before making a diagnosis of primary idiopathic frosted branch angiitis, infiltrative disorders such as leukemia and lymphoma, infective causes such as cytomegalovirus retinitis, and diseases such as Behcet's and sarcoidosis, which may cause widespread vasculitis, should be ruled out. It is responsive to corticosteroid therapy and prognosis is good with timely intervention.

REFERENCES

1. S Walker1 , A Iguchi, NP Jone, 2004. Frosted branch angiitis: a review, Eye (Lond). May;18 (5):527-33.
2. Abhay Gupta, V. K. Anuradha, 2017. A Case of Frosted Branch Angiitis, Tamil Nadu Journal Of Ophthalmic Science and Research, Volume 55 (3), Page 223-224.
3. Elisabetta Miserocchi, M.D. Frosted Branch Angiitis, 2000. The Ocular Immunology and Uveitis Foundation,Vol. V No. 2.
4. Stephani L. Sugin M.D. Dal E. Henderly M.D. Scot M. Friedman M.D., Le M. Jampol M.D. an J Willia Doyle M.D. 1991. Unilateral Frosted Branch Angiitis, American Journal of Ophthalmology, 111:682-685.
5. Janet Leath Alexander MD, Marijean Miller, 2014. A case of frosted branch angiitis in an immunocompromised child, Journal of Association for Pediatric Ophthalmology and Strabismus, Volume 19 (1) Page 75 – 76.
6. Y Watanabe, 1987. A case of frosted branch angiitis, British Journal of Ophthalmology, 71, 553-558.

The International Journal of Medicine and Sciences ***4*** *(1) 2019 : 33-36*

Case Report

CLADOSPORIUM CONJUNCTIVITIS– A RARE ENTITY

Stella Sinnappan[1,2], Jemaima Che-Hamzah [2], Chandramalar T. Santhirathelagan *[1]

[1]Department of Ophthalmology, Hospital Sungai Buloh, Jalan Hospital, 47000 Sungai Buloh, Selangor, Malaysia.
[2]Faculty of Medicine, University Kebangsaan Malaysia Medical Centre, Jalan Yaacob Latif, Bandar Tun Razak, 56000 Kuala Lumpur, Malaysia.

ARTICLE INFO

Corresponding author:
Dr. Chandramalar T. Santhirathelagan

Email address:
chandramalarhsb@gmail.com

Received:
March 2019
Accepted for publication:
June 2019

Keywords:

Fungal conjunctivitis
Cladosporium
anti-tuberculosis therapy

ABSTRACT

A 61-year-old Malay lady with underlying hypertension presented with right eye pain, redness, swelling and discharge of two weeks duration. She denied preceding trauma or constitutional symptoms. Vision on the right eye was 6/12, ph same and left eye was 6/9. The right conjunctiva was injected with generalized chemosis and presence of follicles. The cornea was clear, anterior chamber was quiet and funduscopy was normal. Left eye examination was unremarkable. The clinical presentation was suggestive of bacterial conjunctivitis and the patient was prescribed topical antibiotics. By third week of follow up, the chemosis had worsened, and we proceeded with CT scan orbit and brain which shows no significant findings. Parinaud ocular-glandular syndrome was suspected as she developed right submandibular lymphadenopathy. She was then given a course of systemic Doxycycline and topical Gentamicin eyedrops. Laboratory investigations revealed leucocytosis, elevated ESR with positive Mantoux test and Bartonella IgM serology but MTB PCR was negative, hence treated as presume right tuberculous conjunctivitis with antitubercular therapy. However, the conjunctival biopsy revealed acute on chronic conjunctivitis with positive fungal culture for Cladosporium sp. A diagnosis of Cladosporium conjunctivitis was reached necessitating systemic Itraconazole and topical fluconazole with discontinuation of antitubercular therapy to which the patient favourably responded. In conclusion, fungal infection of the conjunctiva is rare and may mimic bacterial conjunctivitis and occurs mostly in patients with a weakened conjunctival defence mechanism. Early diagnosis and treatment are crucial to prevent vision-threatening complications.

INTRODUCTION

Acute conjunctivitis is one of the most common cause of eye pain and redness and is most frequently caused by virus or bacteria. Although fungal infection of the eye is considered an important cause of significant loss of vision when typically involving the cornea, sclera and retina, the prevalence of fungal conjunctivitis is low [1].

Candida sp and *Sporotrichum schenckii* has been reported to cause conjunctivitis by A. Lupett *et al* and T. Kashima *et al* respectively [2,3]. Conjunctivitis caused by Candida has been described mainly in two age groups, in the newborns and school children as well as in the adults,with the primary infection being localized in the oral mucosa or vagina [2,4]. Conjunctival infections caused by filamentous fungus are very rare and not frequently diagnosed and published. *Sporotrichum schenckii* was reported in Japan with the diagnosis made by histological study of the bulbar conjunctiva.

We report this unusual case of Cladosporium conjunctivitis to highlight the possibility of mycotic infections in chronic intractable cases of conjunctivitis.

CASE REPORT

A 61-year-old Malay lady with underlying hypertension presented with complaints of right eye pain, redness, swelling and discharge of two weeks duration. There were no other associated symptoms such as blurring of vision or floaters. She had no preceding trauma or constitutional symptoms such as loss of weight, loss of appetite, fever or upper respiratory tract infection. On examination, the best corrected visual acuity was 6/12 in the right eye, and 6/9 in the left eye. Intraocular pressures were within normal range in both eyes. Both pupil were

equal and reactive. Anterior segment examination revealed injected conjunctiva in the right eye associated with severe chemosis. There were follicles presence in the upper and lower palpebral conjunctiva.The extraocular muscles movements were full (Figure 1 and 2). The cornea was clear, anterior chamber was deep and quiet. Both fundi were normal. Left eye examination was unremarkable.

Topical antibiotics chloramphenicol was initially prescribed for presumed right bacterial conjunctivitis. After two weeks the antibiotic was changed to gutt. ciprofloxacin as no improvement observed. The chemosis worsened and there were limitation of extraocular movements. A computed tomography (CT) scan of orbit and brain done to rule out carotico-cavernous was normal. The diagnosis was then revised to Parinaud ocular glandular syndrome as she developed right submandibular lymphadenopathy. She was immediately started on oral Doxycycline 100mg twice daily and topical Gentamicin.

Hematological investigations revealed leucocytosis, raised erythrocyte sedimentation rate, a significantly positive Mantoux test, however Mycobacterium tuberculosis polymerase chain reaction was negative (MTB PCR). Bartonella IgM serology was also positive.

Conjunctival biopsy was then performed and sent for histopathological examination (HPE, as well as for culture and sensitivity (C&S). While awaiting the result, the infectious disease (ID) team was consulted and anti-tuberculosis treatment was instituted for presumed tuberculous conjunctivitis. Subsequent histopathological examination of the conjunctival biopsy revealed a congested tissue consisting of dense chronic inflammatory cells with scattered neutrophils (Figure 3). Culture of the biopsied specimen grew greenish brown to black and greyish velvety nap, with slightly heaped colony, eptate hyphae, dark and branched conidiophore, which produces two or more conidial chains suggesting of *Cladosporium sp*. The final diagnosis was then confirmed as right Cladosporium conjunctivitis.

The patient was co-managed with the ID team. Systemic antifungal, oral Itraconazole 200mg twice a day, taken after meal with acidic drink to produce high bioavailability and absorption. Topically, anti-fungal eye drops, topical Fluconazole hourly was commenced with simultaneous discontinuation of anti -tuberculous drugs.

Figure 3: shows A. Site of conjunctival biopsy B. Low magnification of the HPE results (Hematoxylin and Eosin stain) C. High magnification of HPE results showing a congested tissue consisting of dense chronic inflammatory cells with scattered neutrophils.

On subsequent follow up, the patient responded well clinically to the treatment with reduction of chemosis (Figure 4) and resolving lympadenopathy. Systemic antifungal therapy was completed for 8 weeks then discontinued whereas the topical antifungal therapy was tapered slowly over a period of six months.

DISCUSSION

Cladosporium sp are ubiquitous mold. It is one of the most common genera worldwide and found in soil, plant litter, plant pathogen, leaf surfaces, old or decayed plants. Cladosporium spores are wind-dispersed and they are often extremely abundant in outdoor air and are also widespread indoors on textiles, wood and moist window sills. It grows at 0°C thus is associated with refrigerated foods (1). Such widely distributed fungi can cause various presentations of illness and infections involving the skin, toenails as well as eyes, sinuses and lung.

Fungal ocular infectious diseases are not frequent, but they are more often described because there are more risky factors like prolonged corticosteroid

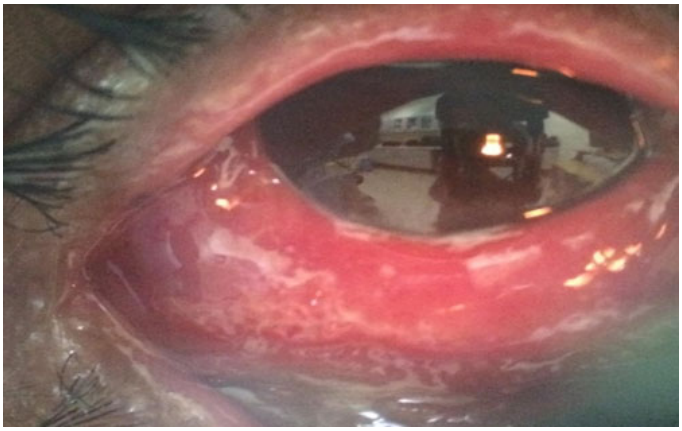

Figure 1: Shows generalised chemosis and redness of the conjunctiva in the right eye.

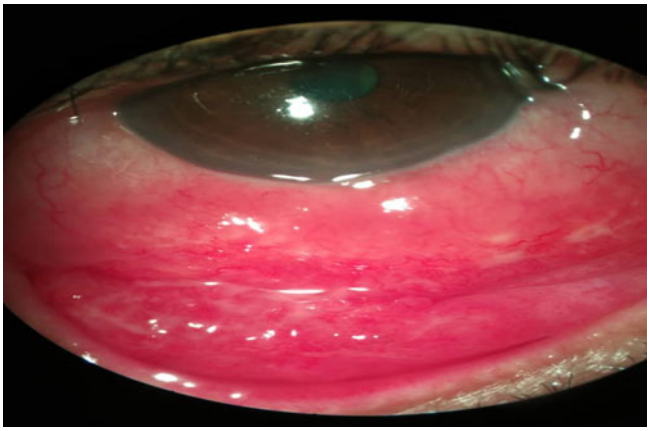

Figure 2: shows follicles in right inferior palpebral conjunctiva.

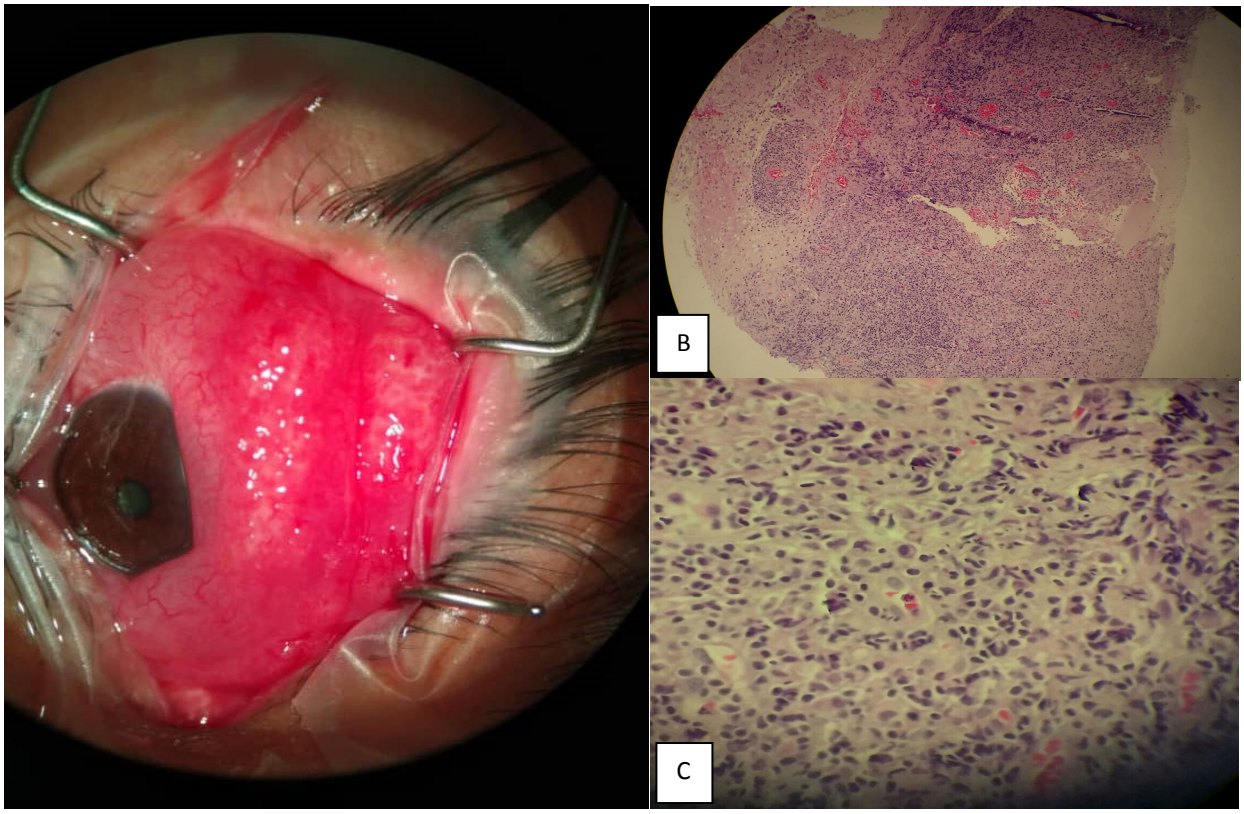

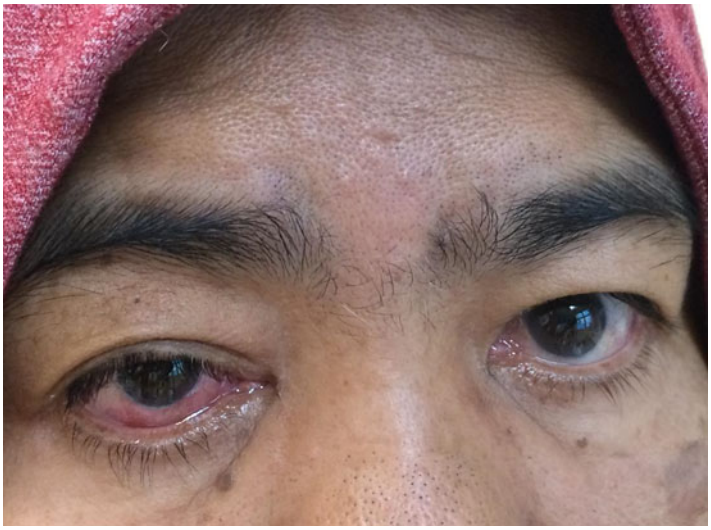

Figure 4: Resolving right conjunctival chemosis at 2 weeks after the systemic and topical antifungal treatment.

treatment or postsurgical long-lasting broad spectrum antibiotic treatment and intravenous drug abuse [5].

Cladosporium conjunctivitis is very rarely reported. Ando N, and Takatori K studied the fungal flora of conjunctival sac in 919 eyes and air-borne fungi [6]. In the study, fungi were cultured from 39 of 587 swabs (6.6%) from healthy conjunctivas. The incidence of positive cultures was significantly higher in diseased eyes (32 of 184 eyes; P less than .005). They found 49 strains of yeast among the 107 isolated conjunctival fungi, including 15 Mycelia sterilia, 12 Cladosporium, and several Aspergillus, Fusarium, and Rhizoctonia species. The air-borne fungi were mainly the filamentous types, especially Cladosporium and Alternaria.

MiroslawSlowik *et al*, reported that fungal conjunctivitis is usually secondary to inflammation of the cornea, lacrimal sac and tear ducts [1]. Candida, Aspergillus, Sporotrichum, Blastomyces, and Dermatophytes (Microsporum, Trichophyton,

Epidermophyton) have also been reported by the author as the etiologic agent causing the symptoms of acute inflammation of the conjunctiva with mucopurulent discharge. He concluded that intensive antifungal therapy is required along with surgical debridement if necessary.

In this patient, worsening of generalized chemosis with significant conjunctival follicles in a unilateral eye as well as associated submandibular lymphadenopathy within 3 weeks of intensive topical antibiotic prompted conjunctival biopsy. The diagnosis was finally arrived from the conjunctival biopsy which revealed acute on chronic conjunctivitis and the culture of the biopsied specimen that grew Cladosporium *sp*. She is a house-wife and revealed later during the treatment that she does gardening occasionally and there was history of exposure to dust from tree bark that entered her eyes prior to symptoms. This could be the predisposing factor.

Hampton *et al* reported a case of conjunctival sporotrichosis in the absence of antecedent trauma [7]. The conjunctival infection in their case resolved completely after excision of the mass and treatment with oral Itraconazole and topical Fluconazole eye drops.

Fungal conjunctivitis is rarely reported and occurs mostly in patients with reduced conjunctival immunity but accidental inoculation of Cladosporium *sp* of the conjunctiva in an immunocompetent patient may occur due to its extreme abundance in the environment. Early diagnosis and treatment are crucial to prevent vision-threatening complications.

CONCLUSION

Fungal conjunctivitis remains rare and post a challenge to ophthalmologist by being resistant for conventional treatment. To have high index of suspicion to a follicular-papillary chronic conjunctivitis with no response to topical antibiotic and a slow evolution is crucial (5). Cladosporium as a cause of conjunctivitis, should be included in the differential diagnosis of chronic conjunctivitis lasting longer than 4 weeks. Systemic Itraconazole and topical fluconazole could be a good choice for treating conjunctival infection by *Cladosporium species*.

DISCLAIMER

There is no any conflict of interest. My research was not funded from any of the following organizations: National Institutes of Health (NIH); Welcome Trust; Howard Hughes Medical Institute (HHMI); and other(s).

REFERENCES

1. Mirosław Słowik, Monika M. Biernat, Donata Urbaniak-Kujda, Katarzyna Kapelko-Słowik, Marta Misiuk-Hojło.Mycotic Infections of the Eye :Adv Clin Exp Med 2015, 24, 6, 1113–1117.
2. A. Lupetti, A. Tavanti, P. Davini et al.Horizontal transmission of Candida parapsilosis candidemia in a neonatal intensive care unit. Journal of Clinical Microbiology, Vol 40, no. 7, 2363–2369, 2002.
3. T. Kashima, R. Honma, S. Kishi, and J. Hirato, “Bulbar conjunctival sporotrichosis presenting as a salmon-pink tumor,” Cornea, vol. 29, no. 5, pp. 573–576, 2010.
4. R. Forte, G. Cennamo, S. D. Prete, N. Napolitano, E. Farese, and A. D. Prete, “Allergic conjunctivitis and latent infections,” Cornea, vol. 28, no. 8, pp. 839–842, 2009.
5. Vanzzini Zago V, Alcantara Castro M, Naranjo Tackman R. Support of the Laboratory in the Diagnosis of Fungal Ocular Infections International Journal of Inflammation.Volume 2012(55): 643104, March 2012.
6. Nobuyo Ando MD, Kosuke Takatori DVM. Fungal flora of the conjunctival sac . American J Ophthalmology; Vol 94,Issue 1, July 1982, 67-74.
7. Hampton DE, Adesina A, Chodosh J. Conjunctival sporotrichosis in the absence of antecedent trauma. Cornea,2002 Nov;21(8): 831-3.

Original Article

MACULA IN UVEITIS PATIENTS: AN OPTICAL COHERANCE TOMOGRAPHY STUDY

Syahrul Bariah Suturi[1], Othmaliza Othman[1], Malisa Ami[1], Norshamsiah Md Din[1], Ropilah Abdul Rahman*[1,2]

[1]Department of Ophthalmology, Faculty of Medicine, Universiti Kebangsaan Medical Centre (UKMMC), Jalan Yaacob Latif, Bandar Tun Razak, 56000, Kuala Lumpur, Malaysia.
[2]Kulliyyah of Medicine & Health Sciences, Universiti Islam Antarabangsa Sultan Abdul Halim Mu'adzam Shah, 09300 Kuala Ketil, Kedah, Malaysia.

ARTICLE INFO

Corresponding author:
Prof Dr. Ropilah Abdul Rahman

Email address:
drropilah@unishams.edu.my

Received:
Apr 2019
Accepted for publication:
June 2019

Keywords:

OCT
Uveitis
Macula edema
Cystoid macula edema
Epiretinal membrane

ABSTRACT

A research was conducted to study the morphology of the macula in eyes of uveitis patients using Optical Coherence Tomography (OCT). Objectives of the study were to describe the morphological characteristic of the macula in uveitis patients using the OCT and to assess the correlation between the foveal thickness and visual acuity. A cross sectional study involving uveitis patients attending the uveitis clinic in Universiti Kebangsaan Malaysia Medical Center. Data collected include age, gender, types of uveitis, visual acuity, macula thickness as measured by the OCT, and fundus photograph. A total of 88 eyes from 88 patients were included in the analysis. Slightly more than half of the eyes (n=47, 53.3%) had no macula edema (ME). Out of the 18.2% of eyes with macula edema, 12.5% had cystoid macula edema (CME) and 5.7% had diffuse macula edema (DME). The remaining 28.4% had epiretinal membrane. There was no statistical difference between subjects with and without ME in terms of age, gender and ethnicity. While ME is present in approximately 20% of eyes with uveitis, there is no correlation between visual acuity and foveal thickness. Poor vision in uveitis has to be accounted for by other causes such as cataract, vitritis and secondary glaucoma.

INTRODUCTION

Uveitis is a leading cause of ocular morbidity in the United States [1]. The causes of visual loss in uveitis patients are numerous. Complications such as cataracts, cystoid macular edema and glaucoma are among the leading causes of reduced vision [2].

Classification and standardization of uveitis is important as it enhances the comparability of clinical research from different centers. There were various classification criteria and inflammation grading scheme as well as outcomes criteria [1,3].

Uveitis may occur with or without accompanying vitritis, retinitis, papillitis, or optic neuritis. Uveitis is classified anatomically as anterior, intermediate, posterior or panuveitis according to International Uveitis Study Group [4].

Macula, a small, oval-shaped, highly pigmented area at the center of the human retina is responsible for central vision. This central 5% of the retina is most critical for vision. The densely packed photoreceptors in the macula control all of the eye's central vision and are responsible for the ability to read, drive a car, watch television, see faces and distinguish details.

Macular edema is the swelling of the macula characterized by an increase in macula thickness caused by fluid leaking from the retinal blood vessels into the macula. Macular edema is the most common macular changes and visual loss associated with uveitis. The abnormal fluid accumulation within the neurosensory retina usually results from the break-down of the inner blood-retinal barrier [3].

Optical Coherence Tomography (OCT) is a non-invasive technology for imaging the multi-layered sensory tissue lining the back of the eye. It is commonly used to image lesions of the macula, such as macular thickening in diabetic macular edema [5,6,7]. Currently OCT is an ophthalmic technology that has been used to image a multitude of retinal diseases. Macular lesion associated with optic nerve head pits, epiretinal membranes, central serous chorioretinopathy, age-related macular degeneration, choroidal neovascularization, diabetic macular edema and uveitis are some of the diseases that have been studied using the OCT [8,9].

The ability of OCT to provide quantitative measure-ment makes it complimentary to traditional means of examination by ophthalmoscope and slit lamp biomicroscopy [3]. Optical Coherence Tomography

was found to be in good agreement with the clinical gold standard (slit lamp examination through a dilated pupil) for detecting the presence or absence of macular edema and was found to be more sensitive in cases of mild foveal thickening [8].

The introduction of OCT has enabled clinicians to reliably detect and measure small changes in macular thickness and to quantitatively evaluate the efficacy of different therapeutic modality [5,10,11]. It has emerged as a useful imaging technique by providing new high-resolution cross-sectional information about various pathology of the macula [7]. It also allows clinicians to quantitatively measure macular thickness in a reliable and highly reproducible manner.

The advantage of OCT imaging is its high resolution, which is on the order of 10 to 15 mm axial direction [11]. Optical Coherent Tomography has been demonstrated to be a valuable technique for the detection and the monitoring of a variety of macular disease in uveitis [5,7].

This study measured and defined macular thickness values in uveitic eyes using OCT mapping software, which is now proven to be an effective non-invasive investigation in detecting macular morphology in uveitis and is an important ancillary investigation at the time of initial diagnosis [11]. The measurements can be repeated safely during follow-up to monitor response to any intervention and treatments (6).

We studied the morphological characteristics of uveitic macula by the OCT and the correlation between the foveal thickness and visual acuity among various types of uveitis.

MATERIAL AND METHODS

This was a hospital based cross-sectional study conducted between December 2009 and May 2010 involving patients diagnosed with uveitis attending the uveitis clinic in University Kebangsaan Malaysia Medical Center (UKMMC).

One eye per patient was selected. Inclusion criteria were consented uveitic patients, clear media for a good fundus photography and good OCT signal strength of more than four. Patients with poorly dilated pupil and media opacity precluding a good OCT image were excluded. Ethical approval was obtained from the Research and Ethics Committee, Faculty of Medicine, Universiti Kebangsaan Malaysia. Written consent was obtained from all participants prior to participation in this study.

Uveitis was classified as below:

Anterior uveitis : affecting the anterior of the eye, mainly the area around the iris.

Intermediate uveitis: affecting the area around the anterior end of the retina and the vitreous.
Posterior uveitis: affecting the posterior portion of the eye including the retina and optic nerve.
Panuveitis: affecting at least two of the disease forms described above.

The mean foveal thickness measurement with OCT is considered to represent the macular as it is the best discriminator between eyes with or without macular morphology such as macular edema. Macular edema is present when the mean retinal thickness at the central fovea was more than 333+171mm [12].

The Optical Coherence Tomography (OCT)
Stratus OCT with a 2 mm deep, 6 mm wide image was used for macular imaging. Imaging was performed at two different transverse scan densities: standard density (high-speed acquisition) and high density (lower-speed acquisition). For each session, the scan alignment was be guided by the fundus image provided by the OCT system. The OCT did not allow additional alignment between visits. The macular scan is composed of six linear scans centered at the fovea equally spaced 30° apart. The entire standard scan types for the fast speed acquisition were attained simultaneously. The OCT images were automatically analyzed with the Stratus OCT software and quantitatively measured the macula thickness by segments [13].

Upon dilatation of the pupils using Guttae Mydriacyl 1% and Phenylephrine 2.5%, macular thickness measurement were obtained using the Stratus Optical Coherence Tomography model 3000. Macular scans consisted of six 6-mm linear radial scans through the foveal in a spoke-like configuration, with each line 30 degrees apart. The macular scan gave average macular thickness values of 9 zones, the inner macular thickness in superior, inferior, nasal and temporal quadrants in μm; and outer macular thickness in the superior, inferior, nasal and temporal quadrants in μm (Figure 1).

Finally, fundus photograph was taken for each subject for photographic documentation using the Topcon TRC 50DX retinal camera.

Visual acuity (VA):
Visual Acuity is the acuteness or clearness of vision. In this study, Snellen chart was used to determine visual acuity. The Snellen acuities were converted to a LogMar scale (Table 1).

Data were analysed using SPSS version 16.0. The value of $p<0.05$ was considered as significant. Data were checked for its normal distribution with histogram, skewness and kurtosis test and Kolmogrove-smirnov test. Spearman's Rank Order Correlation was used to examine the relationship between foveal thickness and visual acuity.

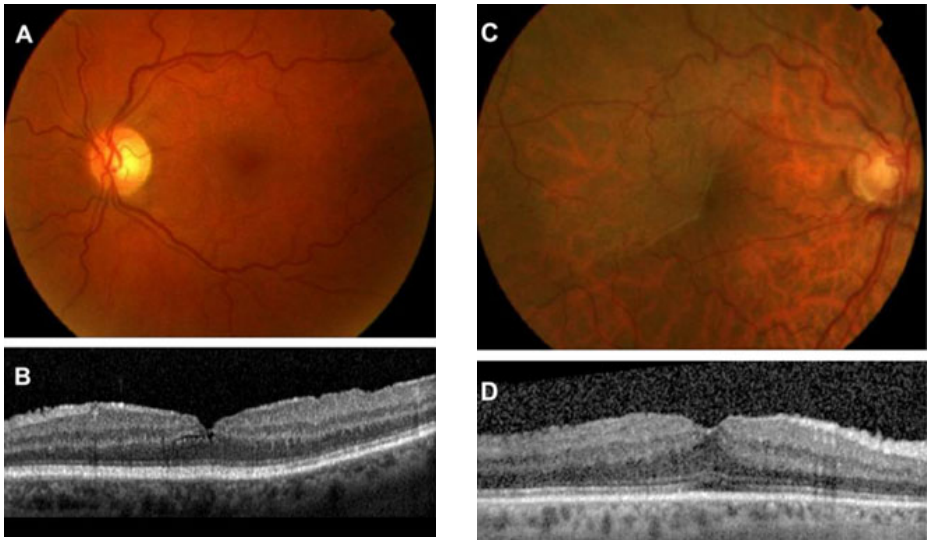

Figure. 1: **A** is Fundus with mild macula edema and **C** the corresponding OCT. **B** is the macula edema with epiretinal membrane and **D** the corresponding OCT.

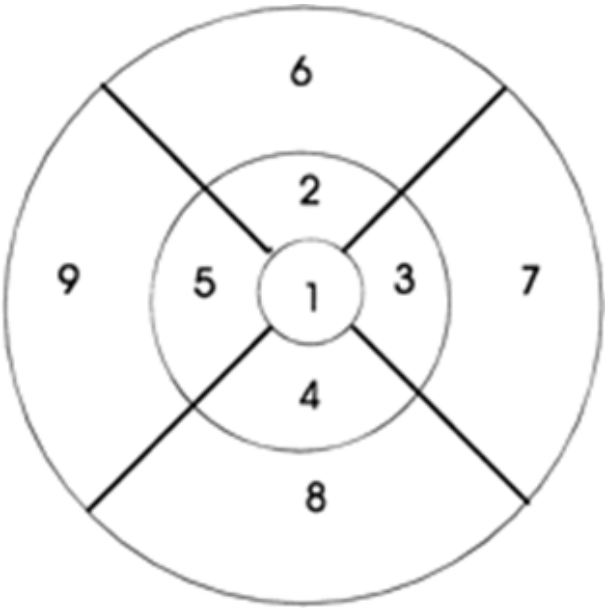

Figure 2: OCT scan of the macula in 9 zones

Table 1: Conversion chart: Snellen verses LogMar.

Snellen (m)	**LogMar**
6/3	-0.3
6/4	-0.2
6/5	-0.1
6/6	0
6/9	0.2
6/12	0.3
6/18	0.5
6/24	0.6
6/36	0.8

RESULTS

Demographic Data

A total of 88 patients were eligible for the study (Table 2). Patients aged 30 - 44-years-old formed the highest number, 31 of 88 eyes(35.2%), followed by the age group 45 – 59-years-old, 21.6%.
Anterior and intermediate uveitis formed the two most common types of uveitis , 36.4% and 34.1% respectively, followed by panuveitis (17%) and posterior uveitis (12.5%).

Morphologic Characteristic of Uveitic Macular

We found 41 out of 88 patients (46.6%) had macular changes (Table 3). There were 3 patterns of macular thickening identified in this study: cystoids macular edema (CME) (11 eyes, 12.5%) diffuse macular edema (DME) (5 eyes, 5.7%) and epiretinal membrane (ERM) (25 eyes, 28.4%).

Table 4 showed characteristics of subjects with and without macula changes. There was no statistically significant difference between the groups with and without macula changes in term of gender,age and ethnicity ($p>0.005$).

The Correlation between Foveal Thickness and Visual Acuity Among Various Classification of Uveitis

To study the relationship between two entities, we used Spearman correlation as both data were not normally distributed. There was no statistically significant correlation between the foveal thickness and visual acuity within eyes with or without macula changes (Table 5, Figure 3, 4).

Classification of uveitis among age group was showed in Figure 5.

Table 2: Demographic characteristic of the study population.

CHARACTERISTICS	PATIENTS (n)	%
AGE GROUP		
0-14	1	1.1
15-29	22	25
30-44	31	35.2
45-59	19	21.6
>60	15	17
GENDER		
Male	47	53.4
Female	41	46.6
RACE		
Malay	50	56.8
Chinese	33	37.5
Indian	5	5.7
UVEITIS CLASSIFICATION		
Anterior	32	36.4
Intermediate	30	34.1
Posterior	11	12.5
Panuveitis	15	17.0

Table 3: Morphologic characteristic of the macula in the study population.

MACULAR CHANGES	PATIENTS (n)	%
No changes	47	53.4
Cystoid macular edema	11	12.5
Diffuse macular edema	5	5.7
Epiretinal membrane	25	28.4

Table 4: Characteristics of subjects with and without macula changes.

CHARACTERISTICS	NO MACULAR CHANGEs	WITH MACULAR CHANGES	p value
Eyes, n(88)	47	41	
Age Mean	39.55±15.376	43.07±16.837	0.315[a]
Gender Male Female	25 22	22 19	0.96 [a]
Race Malay Chinese Indian	27 (54.7%) 17 (36.2%) 3 (6.4%)	21 (51.2%) 17 (41.5%) 3 (7.3%)	0.843 [a]

[a] Chi-Square test

Table 5: Correlation between foveal thickness and visual acuity.

	No macular changes	With macular changes
Correlation coefficient	0.269	-0.178
p value	0.067	0.266

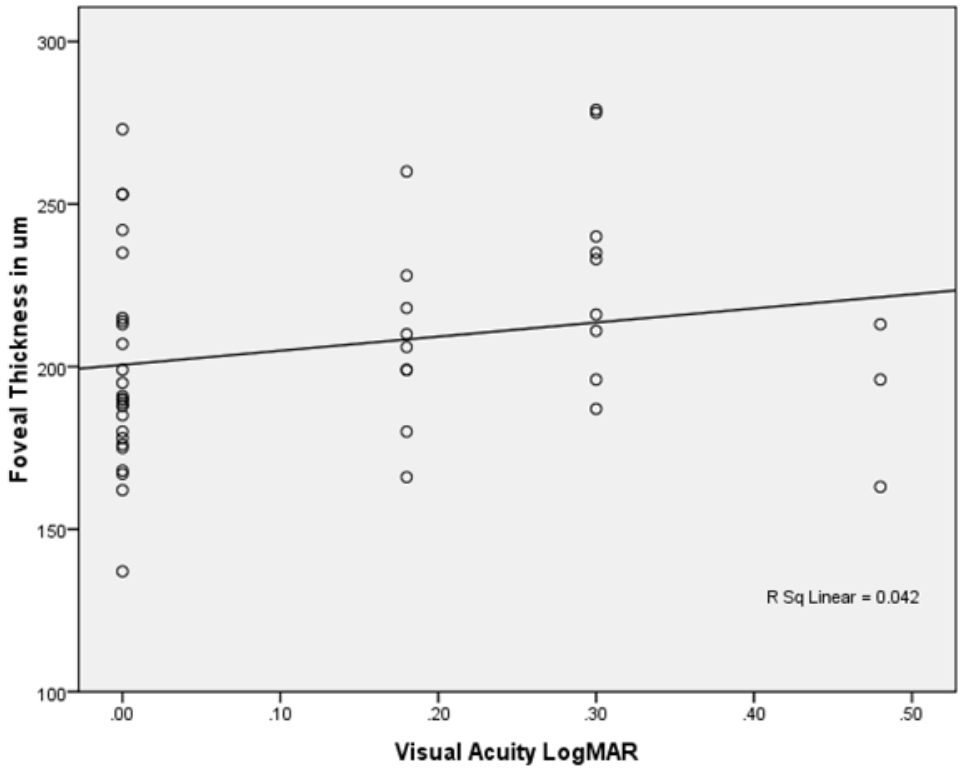

Figure 3: Correlation between foveal thickness and visual acuity in eyes with no macular changes.

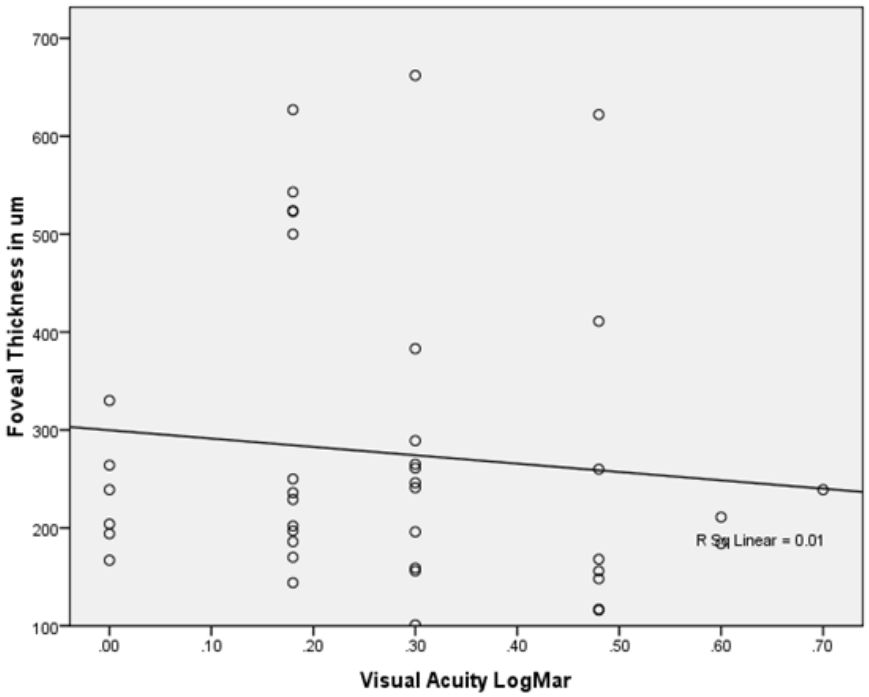

Figure 4: Correlation between foveal thickness and visual acuity in eyes with macular changes.

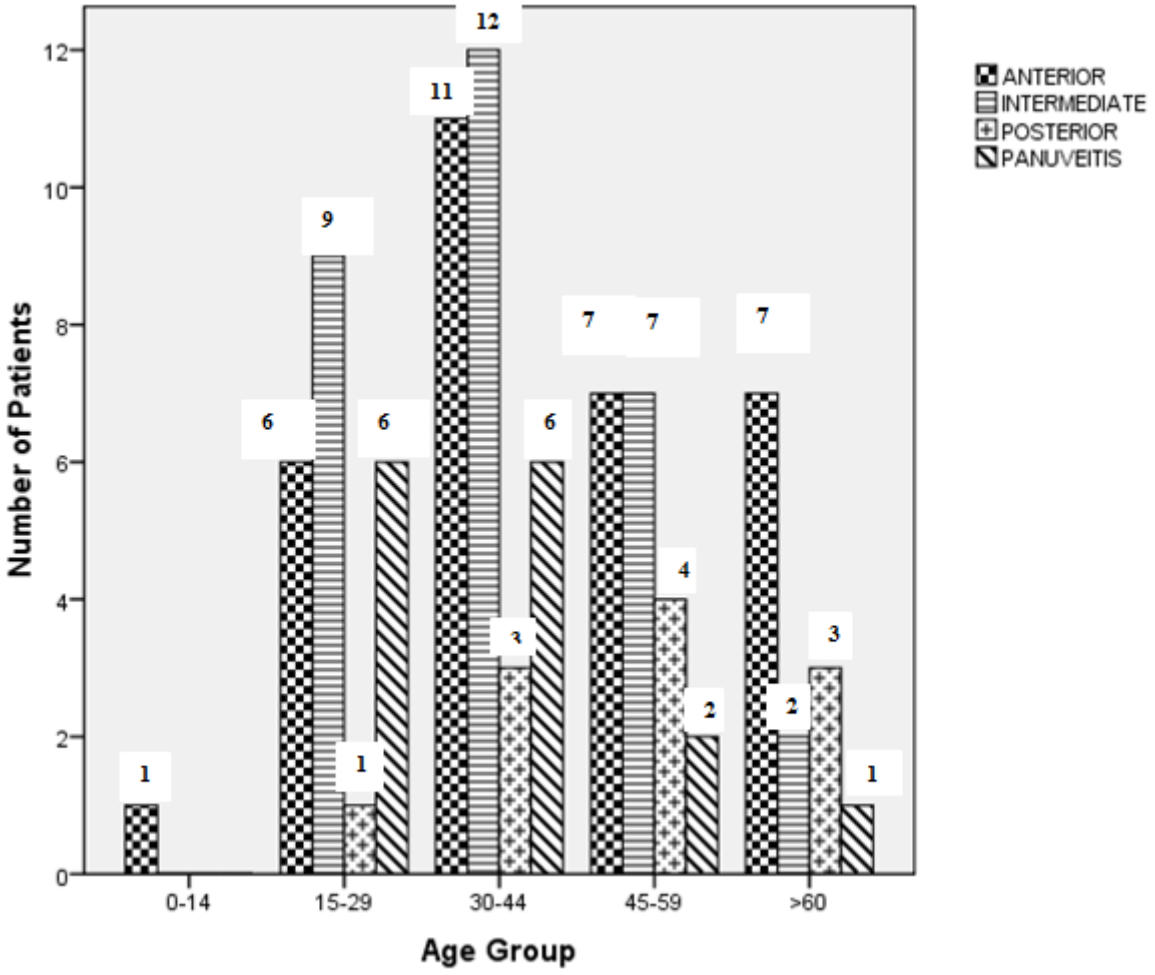

Figure 5: Classification of uveitis distribution among age groups.

DISCUSSIONS

Uveitis is one of a leading cause of ocular morbidity in the United States according to 2001 study by Rhett et al, although population-based estimates of its true incidence and prevalence are not available [1].

Application of Optical Coherence Tomography (OCT) as an imaging modality for non-invasive cross-sectional imaging of the biological tissues was first reported in 1991 by Huang et al [13]. Since its development in 1991, OCT has been investigated in a wide range of clinical applications. This helps in interpretation of pathology in the context of its anatomic location, substantiating the diagnosis, monitoring the course of the disease and evaluating the response therapeutic intervention [4].

The age and gender distribution of patients in this study compares well to other studies, with majority of the patients in the age group 30 – 45 years-old and almost equal male and female proportion [14].

The racial breakdown of uveitic patients was found to be interestingly similar to the racial breakdown of the Malaysia population, according to the population census done in 2000 (65% Malays, 26% Chinese, 7% Indian and 2% others) [14]. This finding may suggest that this disease affects the races equally and has no predilection for any one race in particular.

According to the anatomical classification of uveitis (IUSG) , in our study we found 36.4% (32 eyes) anterior uveitis followed by intermediate uveitis, 34.1% (30 eyes), posterior 2.5% (11 eyes) and panuveitis 17.0% (15 eyes). The similar distribution is seen in study done by Das et al in 2009 [13,15].

In this study, 46.6%, that is 41 out of 88 eyes, had macular changes. Optical Coherence Tomography revealed 3 patterns of macular thickening, CME was detected in 11 eyes(12.5%) and DME in 5 eyes, (5.7%) and ERM in 25 eyes (28.4%). Markomichelakis et al in 2007 described three patterns of macular edema: Cystoid Macular Edema (CME), Diffuse Macular Edema (DME) and Retinal Detachment (RD) however we observed CME, DME and ERM with no evidence of RD [12].

Unlike other studies we found no correlation between foveal thickness and visual acuity in both groups, with no macular changes (r=0.269, p= 0.067) and with macular changes (r = -0.178, p=0.266) [16]. This is probably due various stages of uveitis recruited in our study and other causes of reduced vision such as cataract, vitritis and secondary glaucoma which is beyond the scope of this study [17].

CONCLUSION

Morphological characteristics of macula in uveitis found in this study by OCT are cystoids macular edema (CME), diffuse macular edema (DME) and epiretinal membrane (ERM). There is no correlation between foveal thickness and visual acuity in eyes with and without macular changes. Majority of cases were in the age group 30-44 years-old with Intermediate uveitis being the most prevalent.

FINANCIAL SUPPORT

This study was funded by the Universiti Kebangsaan Malaysia.

CONFLICT OF INTEREST

No conflict of interest exists for any of the authors

REFERRENCES

1. Rhett Schiffman, Gordon Jacobsen, Scott.M Whitcup. 2001. Visual Functioning and General Health Status in Patients with Uveitis. *Arch Ophtalmol*, Vol 119, pp 841-849.
2. Durrani OM,Tehrani NN, Marr JE et al. (2004). Degree, duration and causes of visual loss in uveitis. British Journal of Ophtalmology. Vol 88, pp 1159-1162.
3. Kiss CG, Ausenbauer TB, Saskia M et al. 2006. Reading Performance of Patients with Uveitis-Associated Cystoid Macular Edema. *American Journal of Ophtalmology*. Vol 142 (4), pp 620-625.
4. Bloch ME, Nussenblatt RB. 1987. International Uveitis Study Group: Recommendations for the Evaluation of Intraocular Inflammatory Diseases. *American Journal of Ophtalmology.* Vol 103(234).
5. Chan A,Duker JS, Ko TH, Fujimoto JG. 2006. Normal Macular Thickness Measurements in Healthy Eyes Using Stratus Optical Coherence Tomography. *Arch Ophtalmol*. Vol 124, pp 193-198.
6. Marcus CC Lim,Siek Tien Hoh,Paul J Foster,Tok Han Lim,Sek Jin Chew Steve KL Seah,Tin Aung. 2005. Use of Optical Coherence Tomography to Assess Variations in Macular Retinal Thickness in Myopia. *Investigative Ophtalmology & Visual Science*. Vol 46 (3), pp 974-978.
7. Vishal Gupta, Pawan Gupta, Ramandeep Singh, Mangat R Dogra, Arnold Gupta. 2008. Spectral-Domain Cirrus High-Definition Optical Coherence Tomography is Better than Time-Domain Stratus Optical Coherence Tomography for Evaluation of Macular Pathologic Featured in Uveitis. *American Journal of Ophtalmology*. Vol 145 (6), pp 1018-1022.
8. Annie Chan BS, Jay S Duker. 2005. A Standardized Method for Reporting Changes in Macular Thickening Using Optical Coherence Tomography. *Arch Ophtalmol*. Vol 123, pp 939 -943.

9. Saraiva FP, Patricia GC, Daniela LI, Carlos SNM, John HJ,Yoshitaka N . 2007. Consistency of Ocular Coherence Tomography Fast Macular Thickness Mapping in Diabetic Macular Edema. *Clinics*. Vol 62 (6), pp 721-4.
10. Rui Bernandes, Torcato Santos, Jose Cunha-Vas. 2008. Increased-Resolution OCT Thickness Mapping of the Human Macula: A Statistically Based Registration. *Investigative Ophthalmology& Visual Science*. Vol 49 (5), pp 2046-2052.
11. Paunescu LA, Schuman JS, Fujimoto JG. 2004. Reproducibility of Nerve Fiber Thickness, Macular Thickness, and Optic Nerve Head Measurements Using Stratus OCT. *Investigative Ophtalmology & Visual Science.* Vol 45 (6), pp 1716-1723.
12. Markomichelakis NN, halkiadakis I, Pantelia E, Peponis V, Patalis A,Theodossiadis P, Theodossiadis Gl. 2004. Patterns of Macular Edema in Patients with Uveitis: Qualitative and Quantitaive assessment using Optical Coherence Tomography. *American Academic of Ophtalmology*.Vol 111(5),pp 946-53
13. Huang D,Swanson EA, Lin CP,Schuman JS,Stinson WG,Chang W,Hee MR,Flotte T, Gregory K et al. 1991. Optical Coherence Tomography. *Science*. Vol 254(5035) pp 1178-1181.
14. Department of statistics, Malaysia : population distribution and basic demogragraphic characteristics 2000,http://www.dosm.gov.my
15. Dipankar Das, Harsha Bhattacharjee, Pankaj Kumar Bhattacharyya, Lonkesh Jain, Panicker MJ et al. 2009. Patterns of Uveitis in North East India; A Tertiary Eye Care Center Study. *Indian J Ophtalmology*. Vol 57(3), pp 144-146
16. Hussain n, Parsal A, Khanna R,Hussain A. 2009. Correlation of Foveal Thickness Measured on Optical Coherence Tomography an Visual Acuity in Eyes with Idiopathic Epiretinal Membrane. *The Internet Journal of Ophthalmology and Visual Science*, Vol 7(2).
17. Prieto – Del – Cura M , Gonzalez Guijjarro. 2009 . Complication of Uveitis : Risk Factors in a series of 398 patient. *Hospital de La Princesa, Servicio de Oftalmología, Madrid, España,* Vol 84(10) pp 523-8.

Kulliyyah of Medicine & Health Sciences, Universiti Islam Antarabangsa Sultan Abdul Halim Mu'adzam Shah,
Kuala Ketil Campus, 09300 Kuala Ketil, Kedah Darul Aman.
tijms.editor@gmail.com